The University Of Sheffield.

UNIVERSITY OF LEEDS

MEC6905 Mini Project (group)

Fretting Corrosion in Modular Hip Joints: Critiquing Standard Practice ASTM F1875

Rachel **BINGLEY,** Olivia F. **MANFREDI,** Alan T. **MARTIN,** Mahdiyar **NEJADHAMZEEIGILANI,** Muhammad Sohail **SIDDIQUI**

January 2014

Prof. Anne N. Neville, Dr. Michael G. Bryant

A report submitted by iT-CDT students from the University of Sheffield and the University of Leeds

GLOSSARY OF TERMS AND ACRONYMS

ASTM	American Society for Testing and Materials
THA	Total Hip Arthroplasty
UHMWPE	ultra-high molecular weight polyethylene
FEA	finite element analysis
SEM	Scanning electron microscope
MoM	Metal-on-metal hip replacement
CoM	Ceramic-on-metal hip replacement
CoC	Ceramic-on-ceramic hip replacement
LC CoCr	Low carbon cobalt-chromium-molybdenum
Cone, Taper, Trunnion	Names used in the literature for the tapering circular cross-section of a modular femoral stem which attaches mechanically to a modular femoral head
Bore	The tapered hole in a modular femoral head which attaches mechanically to a modular femoral stem
FBS	Foetal Bovine Serum
PBS	Phosphate Buffered Saline solution
EDXS	Energy Dispersive X-ray Spectroscopy

CONTENTS

TABLE OF FIGURES

TABLE OF TABLES

ACKNOWLEDGEMENTS

The authors would like to thank their supervisors; Anne Neville and Mike Bryant, for their support throughout the project. Other people who have contributed expertise and are also thanked are Abimbola Oladokun, Michele Schirru and Andrew Beadling. University staff who provided support are also thanked, including; Steve Caddick, Tony Weisse, Ron Cellier, Jordan Thomas, Stuart Mickelthwaite, Andrew O'Brien, Dave Boyes, Darren Trowsdale, Lee Wetherill and Kim Matthews.

1. INTRODUCTION

A Total Hip Arthoplasty (THA) is the operation to remove a damaged human hip joint and replace the load bearing surfaces artificially. Damage could be from an injury or a debilitating condition such as osteoarthritis. These operations are becoming more common with an aging population but also more common in younger, more active patients. This has seen the lifetime demands placed on total hip replacements (THR's) increase from the ~10 year lifecycles originally deemed acceptable for a 60+ year-old patient. The first (Charnley) designs of THR's were relatively simple and effective, but later designs have become more complex in response to the greater expectations put on them and with the incremental increase in knowledge via research. The development of modular THR's was driven by wear occurring between the femoral head and the acetabular cup. A modular femoral head could be excised and replaced should it wear prematurely, leaving the femoral stem in place in the patient's bone. The current study focuses on metal-on-metal (MoM) modular hip replacements, particularly the interface between the bore of the modular femoral head and the cone of the modular femoral stem, referred to as the taper interface.

Fretting-corrosion is the synergy of mechanical fretting wear and chemically induced corrosion, and has been found to occur in the taper interface. ASTM F1875 is a test standard intended to provide a benchmark set of tests which manufacturers can use to quickly compare design iterations when developing metal modular femoral stems. A standard test method would also allow researchers to compare results more readily if they test under the same set-up and conditions. However the standard itself is poorly structured and suggests testing solutions which may not be representative of the in vivo environment.

The purpose of this study is to conduct tests according to ASTM F1875 with the intention of testing its clinical relevance. Suggestions for improving the standard will be made, and future work will aim to test these suggestions.

Components investigated include DePuy high nitrogen stainless steel femoral stems and DePuy low carbon cobalt-chromium-molybdenum (LC CoCr) femoral heads. There is little information in the literature from other researchers who tested this material combination. In addition to the ASTM F1875 tests, a ball-on-flat fretting-corrosion test will be conducted as a means of producing and comparing fretting regimes; being a faster, simpler test with more

control over parameters. Explanted THR's will also be examined, to compare the damage in vivo conditions cause to the damage caused by simulated conditions in the lab.

1.1 Aim

The aim of the project is to investigate the interaction of joint fluid on fretting, corrosion and wear in the femoral stem and femoral head interface of a modular hip joint. Objectives of the study are:

- Compare and contrast the two test methods detailed in ASTM F1875 by critiquing the standard and conducting both experimental methods
- To design a tribological test and manufacture relevant apparatus to compare the two test methods
- Determine contact mechanics parameters by means of a FEA
- Compare lubricant formulations, as two are suggested in ASTM F1875 along with a third in ISO 14242, to determine a standard lubricant for use in bio-fretting tests
- Determine the most applicable surface imaging technique, as ASTM F1875 recommends the use of both SEM and optical microscopy to characterise the surface
- Calculate the "total amount of metal release" ASTM F1875 stipulates by: the measurement of corrosion and wear debris due to corrosion via ICP-MS, the measurement of physical wear via CMM, and the measurement of tribocorrosion via mass loss compared with ICP
- Compare experimental damage to explanted components to determine the most applicable lubricant formulation, test method and analysis methods

1.2 Summary of ASTM F1875

Fretting corrosion mechanism is one of the main concerns generally in total hip prosthesis and specifically in the modular headcone interface. Fretting corrosion can generate particulate debris, which weakens the strength and mechanical stability of the femoral stem and ultimately results in the fracture of the neck and also contributes to prosthetic osteolysis [1][2].

There are some ASTM standards which describe the analytical techniques and reference testing methods to evaluate the mechanical stability of bore and cone interface by measuring the localized fretting corrosion [3]. ASTM 1875 is the standard practice for Fretting corrosion testing of modular implant interfaces [3]. This practice basically describes the testing methods which include the analytical and characterization methods for the evaluation of fretting corrosion mechanism and the mechanical stability of the head cone interface of modular hip implant. For evaluating the fretting corrosion mechanism two methods are described in this standard i.e. Method 1 and Method 2 [3].

The basic purpose of method 1, which prescribes a long term test, is to provide a standard set of guidelines to determine the amount of damage by measurement of the corrosion product and debris which are generated as by-products from the fretting corrosion phenomenon[3][1]. This method simultaneously evaluates the fatigue strength of the stem in conjunction with standard practice F1440 (i.e. standard practice for cyclic fatigue testing of metallic stemmed hip arthroplasty femoral component without torsion) and the debris produced by fretting corrosion. A servo hydraulic machine (Instron) is used for mechanical testing purpose and the stemmed femoral components are loaded cyclically as mentioned in practice F1440 [3], as shown in Figure 1-1.

Figure 1-1 - Complete assembly of method I (adapted from [1]**).**

The head cone interface of total hip prosthesis (THP) are subject to micro motion that ultimately results in fretting corrosion, because the head neck junction is exposed to saline (0.9 % sodium chloride (NaCl) in distilled water) or a proteinaceous solution inside an

environmental containment chamber by immersion of the entire device. The head cone interface is enclosed in an elastomeric sleeve, having electrolyte solution surrounding it, but the contact area between the femoral head and low friction thrust bearing is not exposed to the electrolyte solution, as shown in Figure 1-2.

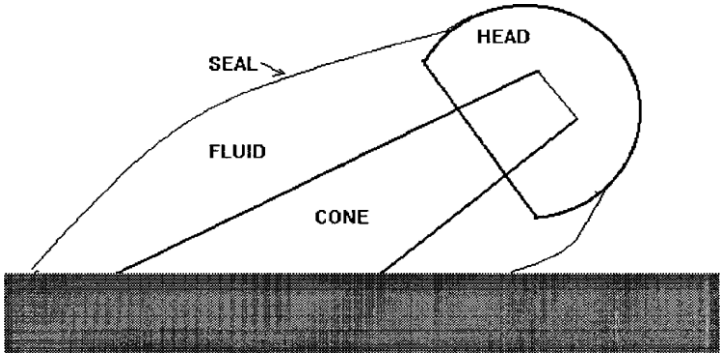

Figure 1-2 - Method 1 pictographic representation of rig set up (adapted from[3]**).**

The volume of the containment is between 5 and 100 ml. The tests are performed with the following criteria:

Test Parameter	**Value**
Single Static load:	2 kN
Maximum cyclic load:	3 kN
Fluid temperature	37 degree centigrade
Minimum cyclic load:	0.3 kN
Frequency	5 HZ
Number of Cycles	500 000

Table 1-1 - Test parameters.

After completion of the test, fluid should be analysed for total metal content and particle characterization as according to practice F561 [3]. After the testing, the surface is inspected for fretting wear and corrosion using optical microscopy and scanning electron microscope. The outcome of method 1 is the quantitative analysis of total elemental level and qualitative analysis of surface wear and corrosion of head cone interface [3].

Method 2 provides the short term electrochemical analysis of fretting corrosion of the head cone interface of the hip prosthesis. The femoral stem and head component similar to Method

1 are mounted in an inverted position rather than upright position as in Method 1. The environmental chamber is filled with electrolyte solution to a sufficient level to submerge the head cone interface and small portion of the neck as well. An elastomeric seal is used to separate the contact area between the femoral head component and the load application surface. The Counter electrode and reference electrode is included in this method for the measurement of corrosion currents and the corrosion potential of the test specimen. Method 2 comprised of two procedures i.e. procedure A and procedure B [3].

In procedure A, a counter electrode along with the saturated calomel electrode with luggin probe or salt bridge is used as a reference reference electrode, which measures changes in corrosion potential with the help of an electrometer. The polarization characteristics are measured with a potentiostat, as shown in Figure 1-3 [3].

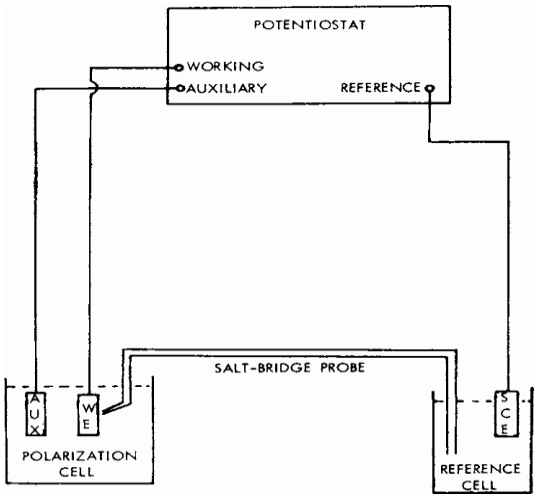

Figure 1-3 - Wiring diagram of electrochemistry rig.

In procedure B, a counter electrode is immersed in the solution and an ammeter is connected between the test specimen and the counter electrode. Difference in current measured before and during cyclic loading shows the fretting corrosion current between the specimen (anode) and the metal bar/sheet (cathode), as shown in Fig. 4 [8]

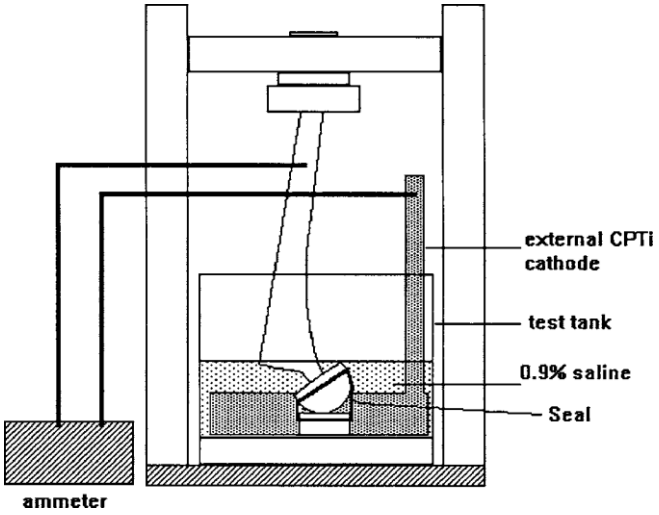

Figure 1-4 - Method II procedure B, set up for measuring fretting corrosion current (adapted from[3]**).**

2. LITERATURE REVIEW

2.1 Hip Arthroplasties

THA is the final solution to severe osteoarthritis. Osteoarthritis is a disease which causes dramatic reduction in articular cartilage thickness on interfacing joint surfaces. The body is unable to replicate articular cartilage and so this condition is progressive and typically results in bone on bone contact. Since bone has effective nerve throughout this leads to extreme pain and limited mobility[4]. There are two main surgeries performed to alleviate this pain in the hip joint, total joint replacement and partial joint replacement/resurfacing. Total joint replacement requires the removal of the damaged joint interfaces and their replacement with artificial versions. This practice is widely accredited to John Charnley, in November 1962, however there were less successful attempts conducted dating back to 1891. Charnley created the metal on polymer implant style still used today, he utilised a stainless steel stem with a polyethylene acetabular cup.[5]

Figure 2-1 - An image of a Charnley Hip Design [6].

Other implant material combinations include other metals on polymers, ceramics on polymers, metals on metals, ceramics on ceramics and metals on metals. There was an increase in metal on metal implantations since 2000, however this peaked in 2006 and since 2008 has seen a decrease to less than 0.1% of primary surgeries in 2013. It has proven difficult to create hip prostheses which are capable of out-performing the Charnley design implants, many of which are still functioning well at 30 years post-op (78%) and some were even still functional at 40 years post-op. That having been said there is evidence for the mechanical superiority of ceramic on polymer and ceramic on ceramic implants, however up to 20% of these suffer from an audible squeaking during use, resulting in patient complaints [7].

The number of hip replacement surgeries increases each year. For the period 2013-2014 there were 620,400 primary hip replacement surgeries completed. Of these the most common bearing surface combination was metal on polymer and the most common fixation type was cemented. These are unsuitable for younger patients and whilst there is evidence that such implants can survive for long periods in vivo this is with primarily inactive subjects. Therefore as patients live longer and can need an implant sooner in life the probability of requiring a revision surgery is increased. There are many studies into different THA designs which attempt to determine the optimum material and geometry designs to increase patient

comfort and mechanical capabilities without having an adverse biological effect. There is also a completely different design, using separate components which enable the easier replacement of damaged parts, without the need for a total removal of the fixed parts. These are called modular hip arthoplasties (MHA). [5], [8]

2.2 Modular Hip Arthroplasties

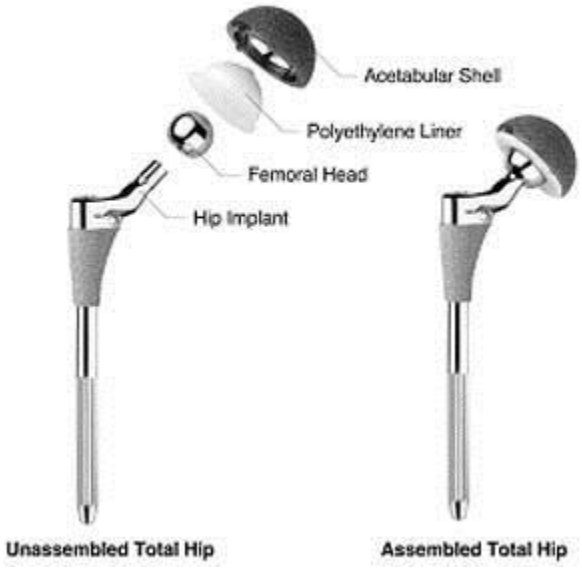

Figure 2-2 - Modular Hip Replacement illustrating the components that compose a standard modular device [9]

As stated above MHA's are when the replacements are made up of multiple components, not just femoral portions and cup sections. They usually consist of removable femoral heads and replaceable acetabular inserts (or liners). The stem and the acetabular cup are both either cemented or otherwise bonded to the underlying bone. MHA's are designed such that these elements are unaffected if a revision surgery becomes necessary, therefore they are designed to be long lasting. Currently the only materials that can support the mechanical loads that such elements require are made of metals, typically either stainless steel or cobalt chromium alloy although there are also titanium alloy stems available. The femoral head has to transfer this mechanical load from the acetabular cup and so is typically constructed of either a metal or a ceramic.[5]

The most common metal used is cobalt chromium alloy although stainless steel has been used in the past and is still within some patients. The most common ceramics in use are alumina and zirconia, and there are some hybrids such as zirconia toughened alumina. These are all

designed to fit with corresponding stems, meaning that if a revision was required a different material head could be inserted, providing it had the same geometry as the initial head. The acetabular lining can be a metal, a ceramic or a polymer, traditionally a polymer was used, based on the Charnley design, although more recently hard materials have been successfully interfaced with other hard materials. The polymers used are usually either UHMWPE or cross-linked polyethylene (XLPE). These are selected due to their low chemical reactiveness meaning they are easier to sterilise and they are biologically inert. The following table shows the common materials for each component.[5]

Component	Material class	Most used material
Femoral stem	Metal	CoCrMo-wrought, Ti-alloys, stainless steel
Femoral head	Metal	CoCrMo-cast, stainless steel
	Ceramic	Alumina (pure or zirconia-toughened), zirconia
Acetabular cup liner	Polymer	UHMWPW, XLPE
	Metal	CoCrMo-cast
	Ceramic	Alumina (pure or zirconia-toughened), zirconia
Acetabular cup shell	Metal	Commercially pure titanium, stainless steel

Table 2-1 - A summary of different materials used in modular hip replacements [5]**.**

2.3 Fretting Corrosion and Wear

2.3.1 Corrosion and Tribocorrosion

Corrosion is the electrochemical oxidation of a metallic material resulting in gradual deterioration of the surface, which is dependent on the rate of the anodic and cathodic reaction[10]. Materials form an oxide passive layer usually between 2-5nm thick to avoid surface corrosion as the oxidised layer acts as a barrier to the substrate; when this layer is worn away, by abrasion for example, the reactive substrate is left vulnerable to the environment thus permitting potential corrosion of the new, un-oxidised surface[11]. When the substrate reacts with its surroundings due to the removal of the passive layer, this process is known as tribocorrosion[12][13]. S. Mischler describes tribocorrosion as "material deterioration or transformation from simultaneous action of wear and corrosion" and thus its analysis requires chemical and physical requirements[12].

2.3.2 Wear mechanisms

Wear mechanisms which contribute to their failure of THA should be fully understood. Conventional mechanisms of wear include, adhesive wear, the transfer of material from one surface to another mainly due to cold asperity welding at asperity junctions; Abrasive wear,

whereby relatively soft material is ploughed out by either asperities on the counter face harder material, which is also known as two bodied abrasion, or hard particles which contribute to the third component of two bodies abrasion known as three bodied abrasion. Erosive wear is characterised by the impact of relatively hard particles carried by a substrate, which is usually in a fluid form. The wear rate, and thus damage to the surface in this mechanism is proportional to the kinetic energy of the particles. Fatigue wear ensues due to cyclic stress variation over a long period of time, thus fatigue wear may contribute to method 1 within this investigation as this wear mechanism can present itself without direct contact between the surfaces. Subsurface cracks may occur from this creating inclusions, porosity or micro-cracks within the material, which may also contribute to the following mechanism of wear[10].

Corrosive wear occurs when a material interaction occurs in the presence of any corrosive environment; debris from this wear mechanism tend not to adhere to the surfaces and result in debris. In the presence of mechanical wear, the rate of corrosion is higher as the passive layer is removed by motion, thus presenting the substrate reacting to the corrosive environment, thus wear accelerates corrosion. Corrosion wear is therefore a combination of chemical and mechanical interactions which is generally the case for wear mechanisms[10]. In general more than one wear mechanism is responsible for surface damage.

2.3.3 Fretting

Synergy of the above wear mechanisms is frequent, fretting being one of these synergy mechanisms which encompasses adhesive, corrosive and abrasive wear. Fretting is the result small oscillatory motion between two metal surfaces, which produces wear debris in the interfacial region. Due to the small amount of relative motion, debris within fretting wear is thought to remain within this interfacial region, however in the presence of a corrosive environment such as those proposed in ASTM F1875, debris may be contained within the solution. Abrasive wear is promoted by stationary wear particles within the interface, however corrosion is promoted by its removal. The relationship between these mechanisms is complex, however it is fair to ascertain that fretting corrosion leads to loss of dimensional accuracy of interfacial regions.

2.3.4 Methods of Quantifying Wear and Corrosion

As tribocorrosion describes the physical and chemical removal of material it is essential to understand the extent to which each of these contribute to the total wear of the system. Watson et al attempted to quantitatively describe this synergy in 1995[14]. Total tribocorrosion material loss was denoted as T, which was said to be the sum of three other terms, being W, the material loss due to pure wear (in the absence of corrosion), C, the material loss due to corrosion (in the absence of wear), and S, the 'incremental factor' of degradation due to the synergy between wear and corrosion[14]. This relationship can be seen in Equation 2.1. synergism of wear and corrosion was found to account for 24-35% of material degradation, with the greatest percent found in 316 stainless steel. The degree of corrosion responsible for material degradation was found to be small ,only 0.1-0.5%, illustrating the importance of wear in combination with corrosion[14].

$$T = W + C + S$$

Equation 2.1

Limitations with this method however lead to the mechanistic approach, as quantifiable separation of each contributing degradation mechanism were dependant on a number of variable factors in the synergistic approach uncovered a need for a simplistic model[12]. Uhlig has shown that the total loss of volume, is the sum of that lost by mechanical and chemical degradation and thus proposed the mechanistic model for fretting corrosion, as seen in Equation 2.2 [12].

$$V_{tot} = V_{mech} + V_{chem}$$

Equation 2.2

Uhlig stated that V_{mech} represents the volume of material removed by mechanical wear, and V_{chem} represents material loss due to wear accelerated corrosion. Although this method addesses the contributing factors of wear in tribocorrosion, it fails to account for de-passivation and re-passivation of the surfaces and also to accommodate for inevitable variability of contact mechanics. As wear mechanisms progress, third bodies can evolve in the form of particle debris which detach from the contacting surfaces. Third bodies affect tribocorrosion, which can be seen as the mechanical loss of volume described earlier by Uhlig as V_{mech}. The response of third bodies within the contact region has been found to vary depending on the test solution[12].

2.4 Solutions and debris

Damage to the taper interface is quantified by analysis of corrosion products and product debris within the solutions from fretting corrosion simulated within the apparatus. Corrosion products and debris are measured by analysis of the electrolyte or proteinaceous solutions. The electrolyte consists of 0.9% sodium chloride (NaCl) in distilled water. The proteinacious solution is a 10 % (vol/vol) calf serum in 0.9% (wt/vol%) NaCl in distilled water[3]. Both solutions immerse the modular junction to permit the quantification of corrosion products and particulate debris released during the simulation. Wear and corrosion between metal on metal (MoM) implants are understood to have important clinical contraindications.

2.4.1 Lubricants

ASTM 1875 describes the interchangeable use of either the electrolyte solution or the proteinacous solution. It was noted that when assessing the wear characteristics of ultra-high molecular weight poly ethylene (UHMWPE) a polymer previously used as the acetabular cup component of THR, the polymer surface film was dependent upon the lubricant used[15]. The natural lubricant used to lubricate the ball and socket joint of the superior femur and the pelvis is synovial fluid, an aqueous electrolyte solution containing proteins lipids and hyaluronic secreted from the synovial membrane. In regards to the solutions used as the electrolytes within the standard the physical and chemical characteristics of these solutions should be understood in order to assess their effect on tribocorrosion and wear at the interface. Proteins influence the corrosive behaviours of materials in static conditions as accelerated corrosion rates are seen in protein rich environments. Yu Yan et al found that increased corrosion was particularly identified in 316L stainless steel when compared to high carbon CoCrMo[16]. The presence of bovine foetal calf serum reduced corrosion of both materials suggesting the formation of a biotribofilm acts as a barrier to corrosion by providing lubrication to the surface[16].

2.5 Ball-on-flat Tribocorrosion Tests

Baxmann et al used titanium on titanium at a frequency of 1Hz for 6000 cycles, comparing displacements of 10, 25, 50μm and Hertzian contact pressures, p_{max}, of 400, 500, 630, 860MPa [17]. This displacement range was chosen because the authors had reviewed three studies which had all reported (variously) micromotion somewhere within the range of 10-50μm. At the lowest pressure of 400Mpa, they observed all three fretting regimes occur for

the displacement range investigated. The ratio between sliding distance (micromotion) and the applied displacement indicated the transition between regimes. Figure 2-3 shows how this ratio relates to load; a load range of 25-100N (corresponding to 400-630MPa) was required to change regimes.

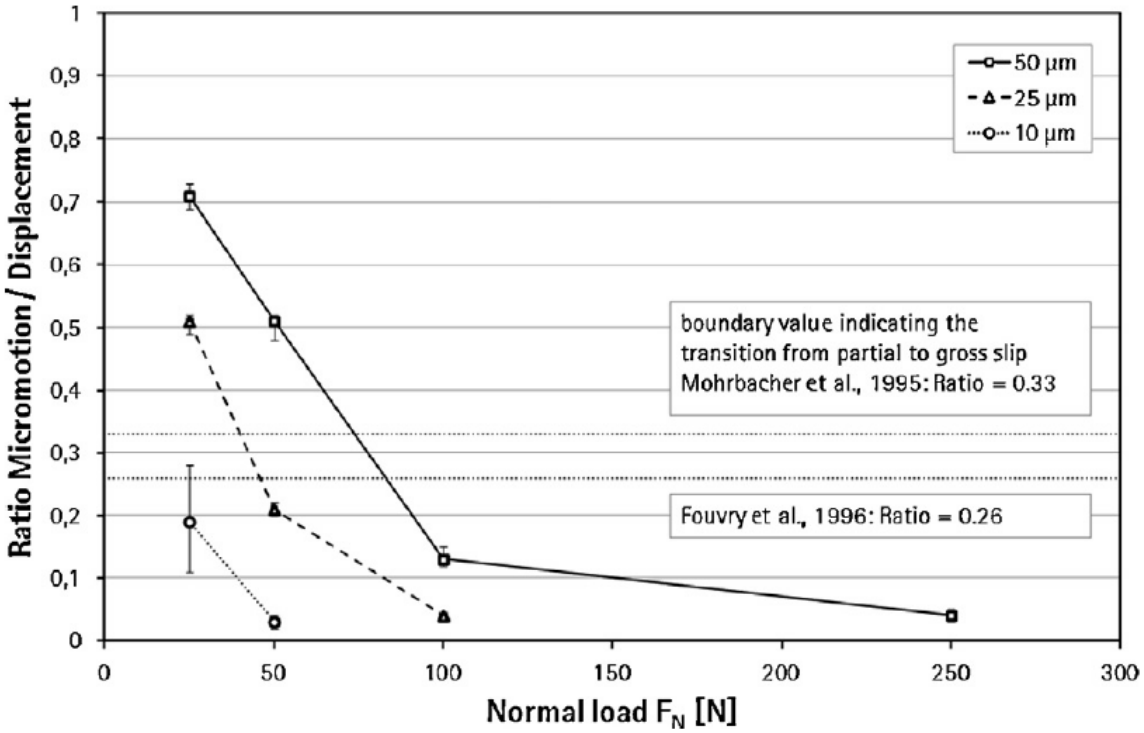

Figure 2-3 - Ratio between sliding distance (micromotion) and applied displacement in relation to load (adapted from[17]**).**

The authors chose the contact pressures following an FEA analysis of the modular stem-neck interface (being the area which they were investigating); basing their loads on data from Bergmann et al's "Realistic loads for testing hip implants" [18]. However Bergmann et al admit their study could be more robust, having only used four subjects to produce the data. Baxmann et al also noted that test frequency was the same as the average frequency of walking.

Barril et al used values of displacement of 3, 10, 30, 50, 100µm and p_{max} pressures of 910, 1314MPa, similar to Baxmann, when studying the effect of displacement amplitude on normal force on Ti6Al4V alloy in contact with an alumina ball [19]. Test frequency was 1Hz, experiments lasted for 3600s. Figure 2-4Figure 2-4 - Several displacement amplitudes are overlaid on the same force-displacement plot for comparison. Tests in (a) were at 910MPa pmax and (b) 1314MPa (adapted from **[19]**).(a) shows some experiments where pressure was

held constant at 910MPa but displacement amplitude varied. For a small deviation in amplitude, the fretting regime can be seen to change: 3µm stick; 10µm stick-slip; >30µm slip. Figure 2-4(b) shows a larger displacement is required to produce similar trends when under a higher constant pressure (1314MPa).

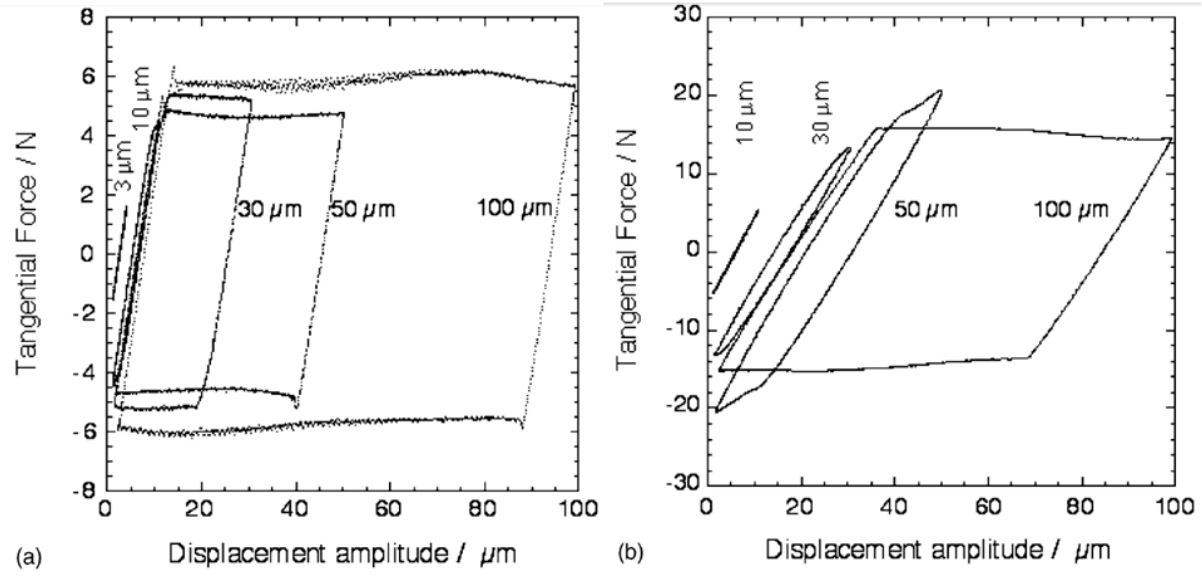

Figure 2-4 - Several displacement amplitudes are overlaid on the same force-displacement plot for comparison. Tests in (a) were at 910MPa p_{max} and (b) 1314MPa (adapted from [19]**).**

It was noted that the stick regime is most prevalent in contacts where the elastic deformation of the contacting surfaces accommodates the majority of the relative motion.

In [20], the authors tested the four different head-on-plate combinations possible with two materials; CoCrMo and Ti -64. Cycle frequency was 10Hz and tests ran for 10^6 cycles. All tests used 50µm amplitude and constant load of 13N (meaning contact pressure would change for the differing material combinations). The authors focussed more on the electrochemistry so do not disclose which fretting regimes were observed.

Runa et al performed ball on plate tribocorrosion tests with a cycle frequency of 1 HZ, applied load 1N, 415 MPa initial Hertzian contact pressure and a stroke length of 2mm during 1800 cycles. The author's state their testing parameters but did not discuss any fretting results, in fact they discussed the electrochemistry in detail [21].

Diomidis et al performed the fretting test with an Alumina ball of 10mm diameter. At cyclic frequency of 1 Hz, they applied normal load of 10N with a displacement of 10 µm during 3600s. An initial Hertzian contact pressure of 400MPa was achieved as a result of the applied load. This fretting corrosion experiment was performed at open circuit and passive potential

and an open trapezoidal shape fretting log diagram showed that fretting phenomenon follows a gross slip regime[22].

Zhang et al conducted an FEA investigation to determine the peak contact pressure found in a cylindrical contact. A 3D model was created, Figure 2-5, to model two slip regimes.

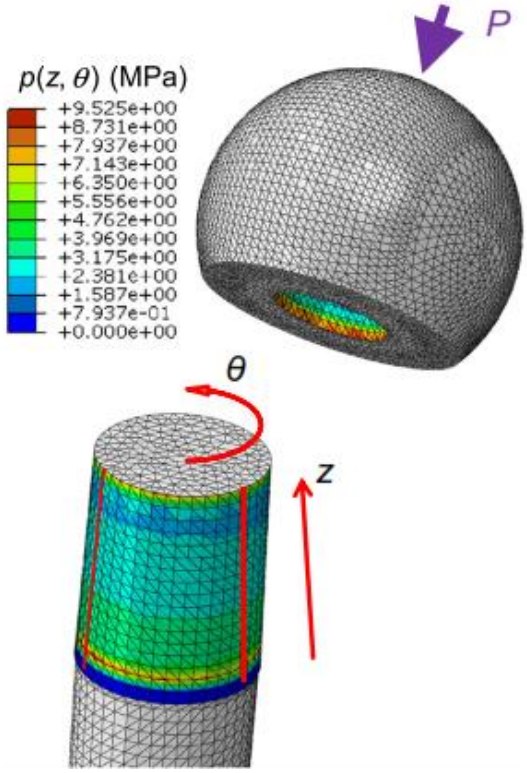

Figure 2-5 - An FEA model of the head-taper interface [23]**.**

The slip regimes investigated were gross slip and partial slip, with a corresponding normal load of 500N and 1000N. The half stroke for the gross slip regime was 40μm and for the partial slip was 22.6μm. Three pin radii were simulated, 3mm, 6mm and 20mm. Figure 2-5 shows that the maximum contact pressure decreased with increasing pin radius.

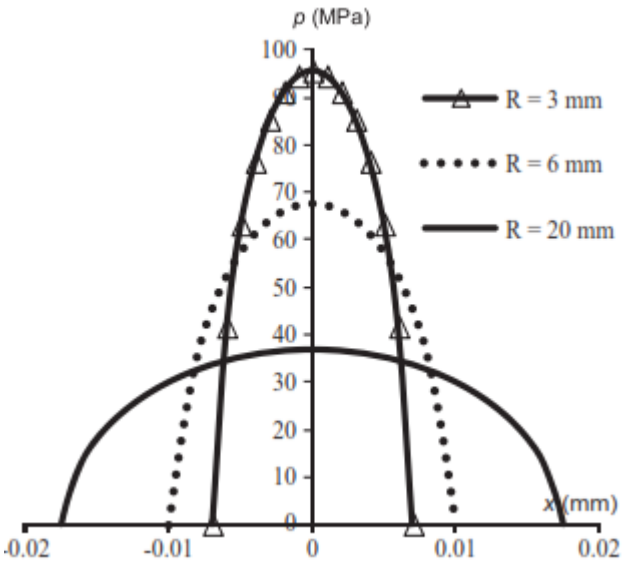

Figure 2-6 - Hertzian solution indicated contact pressure [23]**.**

Zhang et al. then conducted physical fretting tests using a 6mm radius pin to create a maximum contact pressure of 68MPa, which was determined from the FEA analysis results, shown in Figure 2-5 [23].

In summary; there is little to no testing between stainless steel and cobalt chromium head-on-plate tests found in the literature, though a full femoral stem-head system tested by Gilbert et al found greater fretting corrosion in stainless steel/CoCr components than CoCr/CoCr pairs [24]. Baxmann et al and Barril et al found the fretting regimes changed within the displacement range of 3-50μm, or within the pressure ranges 400-630MPa, but this was for modular stem-neck tapers, not stem-head tapers. Zhang et al. used much lower contact pressures for work concerning stem head tapers. It is therefore decided to test with three different displacements; 3, 10, 30μm and at three different Hertzian contact pressures, pmax; 50, 100, 150MPa, since it is unclear where fretting regimes will change for the current study's material combination, but it had changed within these ranges for other material combinations.

2.6 ASTM F1875 Experiments in the Literature

ASTM F1875 makes reference to five research papers. One, by Goldberg et al, uses test procedures which are clear precursors to the two testing methods set out in ASTM F1875 [25]. Another by Jani et al uses a procedure very similar to ASTM F1875 method I [26].

Caminha and Roesler conducted tests in accordance to ASTM F1875 and documented their experimental procedure and rig design neatly [1], although it looks like they used significantly more fluid than the "5-100ml" recommended in ASTM F1875, as Figure 2-7 shows in a photo of their experimental set-up. This design appears more practical than the "elastomeric sleeve" recommended in ASTM F1875 which is used in older studies, particularly when it comes to extracting fluid for later analysis.

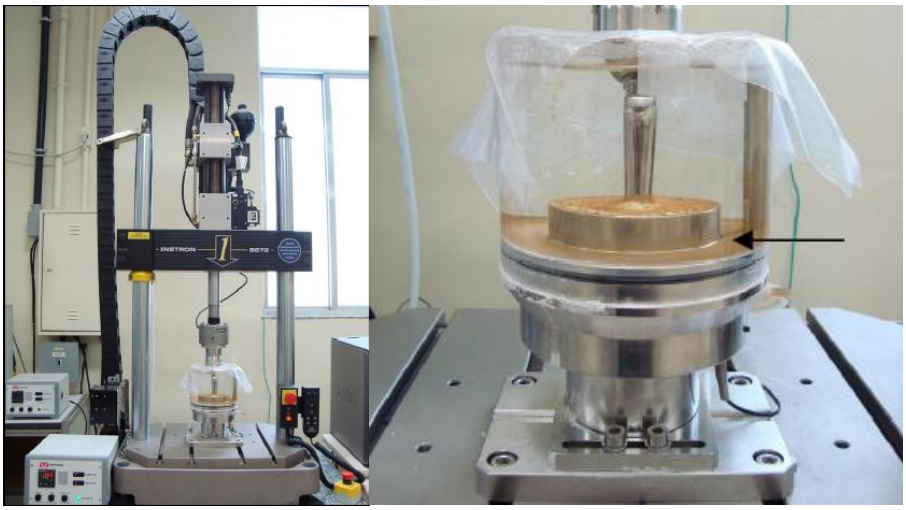

Figure 2-7 - ASTM method I test set-up, also showing significant corrosion product after 10 million cycles (adapted from [1]**).**

Hallab et al [27] cut their femoral stems to form coupons which were cemented in place as per ASTM F1875 Method II Procedure B and ASTM F1440, then used the offcut stem as the counter electrode, as Figure 2-8 shows. Their test procedure differed in that they used 100% FBS and 2Hz loading frequency as "a compromise from lower, more physiological rates to permit a practical testing time period".

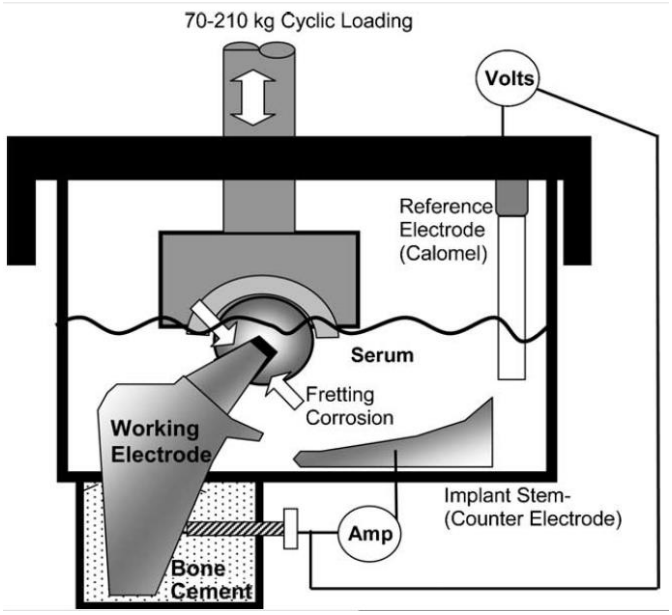

Figure 2-8 - ASTM method II procedure B set-up (adapted from [27]**).**

Other studies have used parameters based on ASTM F1875 Method II, such as Schaaff et al [28], though their set-up was for a sphere-on-plate test. Goldberg and Gilbert tested custom made modular neck taper components against femoral head in a set-up similar to ASTM F1875 method II [2]. The necks had threaded holes manufactured into them to attach to the test rig. The fluid containment method was simple yet effective, as Figure 2-9 shows.

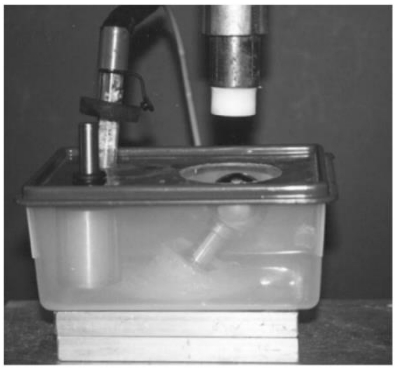

Figure 2-9 - The lunchbox method of containment (adapted from [2]**).**

Gilbert et al use a procedure similar to ASTM F1875 method I but with the inclusion of electrochemistry, and initially increase load to 3300N cyclically from 100N in 100N increments [24]. They also measured relative micromotion between the stem and head using a LVDT sensor, finding it to be in the range of 10-25μm, but to increase with head offset length.

In a previous study conducted at the University of Leeds, a test method was developed based on ISO 7206-4, which is similar to ASTM F1875 Method I [29]. This test rig is available to modify for use in the current study. A new test rig for ASTM 1875 method II will be devised.

3. BALL-ON-FLAT TRIBOCORROSION TESTS

3.1 Parameters

The plate samples were cut from a high nitrogen stainless steel stem (DePuy C-Stem AMT (size 4) standard offset)and mounted in a polymer, then progressively ground and polished to a mirror finish, similar to the typical surface finish of a stem. The constant (circular) cross section of the sample meant its area was simple to calculate for later corrosion calculations. The femoral heads used as the "ball" in the contact are DePuy ARTICUL/EZE M 28MM +1.5, LC CoCrMo in composition.

The test parameters used are summarised in Table 3-1 below.

Table 3-1: Test Parameters

Parameter	**Value**
Displacement	3, 10, 30μm
Max Hertzian contact pressures, p_{max},	50, 100, 150MPa
Equivalent load to be applied (calculated by Hertzian analysis)	0.04, 0.3, 1.02N
Number of cycles	6000
Frequency	1Hz
Solution composition	0.9% NaCl in distilled water, 10% FBS in 0.9% NaCl in distilled water
Material properties (from CES Edupack 2014)	Stainless Steel flat plate: E=200GPa, ν=0.27 Cobalt Chromium spherical heads: E=225Gpa, ν=0.32
Repetitions	3

3.2 Results

Unfortunately at the time of writing tests had not been completed.

4. ASTM F1875 TEST METHODS

4.1 ASTM F1875 Test Methods

ASTM F1875 specifies two separate test methods which utilise separate test specimen orientations, separate test solution compositions, separate loading conditions and separate data analysis techniques. That is to say:

- Method I tests with upright components, Method II inverted;
- Method I specifies a proteinaceous solution of 10% calf serum in 0.9% NaCl in distilled water, Method II uses an electrolyte solution of 0.9% NaCl in distilled water;
- Method I loads the components cyclically between 0.3-3.3kN at a frequency of 5Hz and terminates after 10 million cycles, Method II loads the components cyclically between 40-2040N at a frequency of 1Hz and terminates either when electrochemistry potential becomes stable or when a 3600 cycles are reached;
- Method I analyses results using optical microscopy and a total elemental analysis via SEM; Method II analyses results utilising electrochemistry, which must be validated by a total elemental analysis.

In order to compare the two test methods, the current study will conduct both test methods with both reagent solution compositions and utilising both data analysis techniques. Additional data of fluid viscosity and wear will also be measured via a novel ultrasonic rheometer and mass loss, respectively.

4.1.1 Method I Apparatus

In a previous study conducted at the University of Leeds, a test method was developed based on ISO 7206-4, which is similar to ASTM F1875 Method I [29]. This test rig is available for modification to the current study's needs. A diagram and photo in Figure 4-1 show the test set-up.

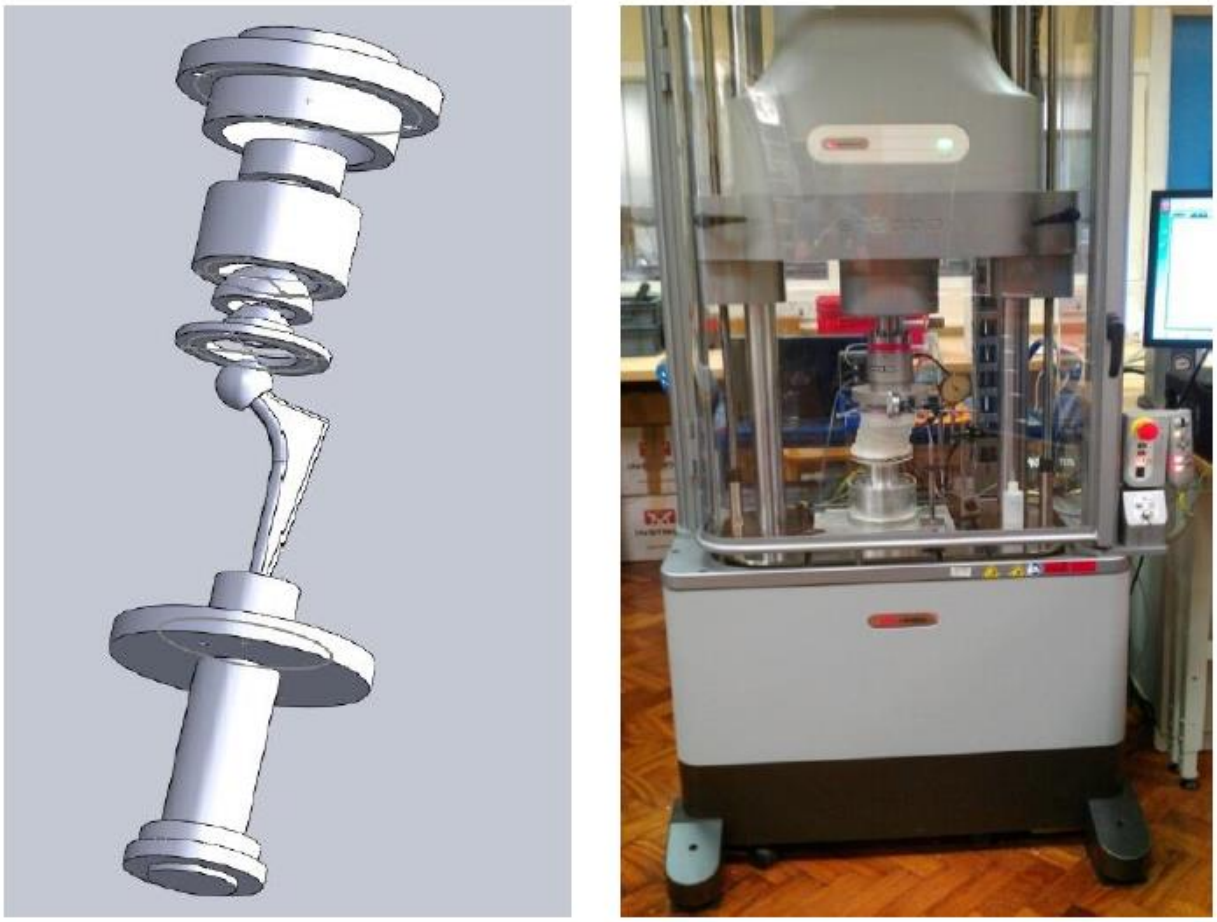

Figure 4-1 – Schematic and photo of the previous upright rig which were modified (adapted from [29]**).**

The load machine is an Instron E10000. Stems used in the current study were high nitrogen stainless steel DePuy C-Stem AMT (size 4) standard offset, heads were LC CoCrMo DePuy ARTICUL/EZE M 36MM +1.5. Most test rig materials in contact with the test solution were bio-inert and non-corroding so as not to affect the sterility of test conditions. Low dose antimicrobials were also used, as recommended by ASTM F1875. ASTM F1875 specifies in section 6.2 “Specimen Mounting Devices, Method I” that “modular hip and stem components shall be set up as described in Practices F1440”. Hence ASTM F1440 section 8.1 details that the components should be mounted at an angle 10° off the line of load application. ASTM F1440 also includes a diagram to illustrate the mounting angle and a design of a suggested gripping device to achieve this angle when setting the stem in a suitable grouting medium, as reproduced in Figure 2-3 here.

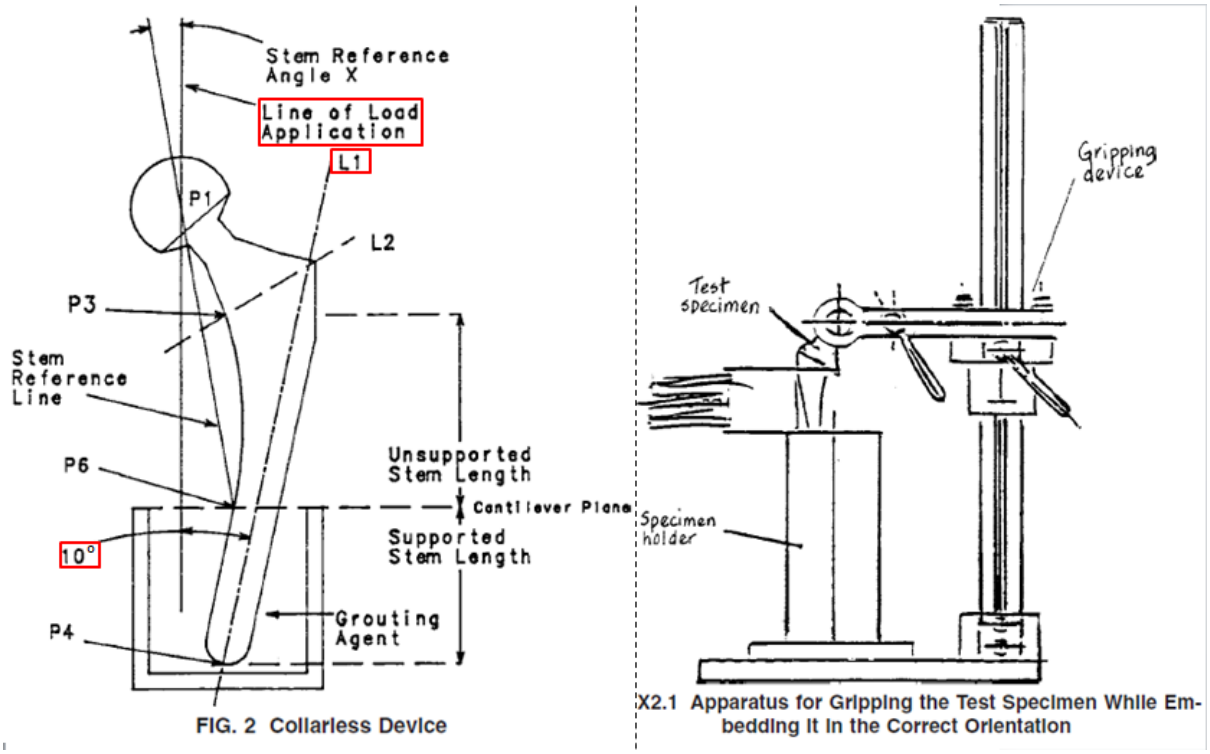

Figure 4-2 - The 10° angle at which the stem should be tested at for ASTM F1875 Method I and a suggested gripping device design (adapted from [30]**).**

The grouting medium used was PMMA bone cement. Silicone sealant was used at the stem-resin interface and the resin-rig interface to minimise undesirable fretting corrosion in areas apart from the head-stem interface. The femoral head is loaded against a component similar in design to an acetabular cup. The femoral heads used in [29] were 28mm in diameter, so the acetabular cup-type component has been redesigned for the current investigations' 36mm femoral heads. The head-cup interface was not immersed so would not be an additional source of fretting corrosion which would require sealing. A silicon gaiter was used to contain the fluid surrounding the exposed stem and head during testing. A thrust bearing was used at the top of the loading configuration to minimise eccentric loads, as bending moments between the head and loading mechanism can affect test results.

4.1.2 Method II Apparatus

The design of the method II test rig was somewhat similar to method I. ASTM F1875 provides little guidance for method II (whereas method I had specified the use of ASTM F1440). Again most materials in contact with the test solution were non-corroding, for example Delrin or Perspex instead of metals; this time to not affect either corrosion or electrochemical analyses employed. Latex free nitrile gloves were used to handle all samples

and any surfaces which came in contact with test fluids, since grease from skin can affect electrochemistry readings. Figure 4-3 shows a schematic of the rig, which includes a thrust bearing at the base of the design to minimise bending moments, although this was not specified in ASTM F1875. Figure 4-3 also shows the O-ring seal design for the immersed loading face in accordance with ASTM F1875.

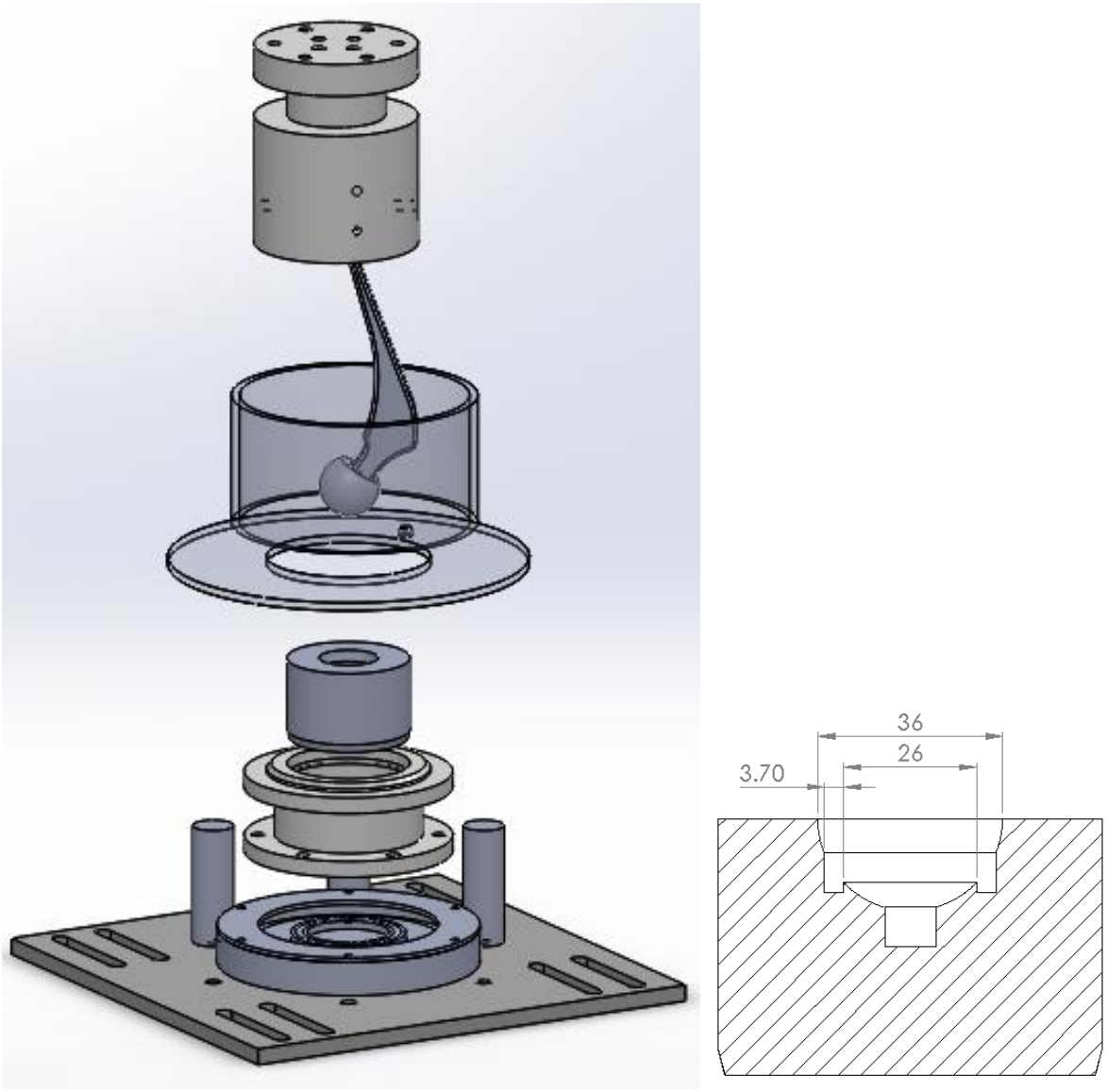

Figure 4-3 – Schematic of the method I test rig manufactured and detail of the seal design at the lower loading face.

5. ELECTROCHEMISTRY

Electrochemical test set up for method 1 and 2 is of similar design apart from the specimen position which is upright in method 1 whereas mounted in an inverted position in method 2 [3]. For measuring open circuit potential the electrochemical corrosion cell utilize only working electrode which is made from femoral stem material (i.e. high nitrogen stainless steel in this case) and Ag/AgCl as reference electrode [31]. The area of working electrode may have impact on the OCP measurements [24]. The Standard experimental test set up for the polarization curve measurement is based on three electrode electrochemical cell. In this arrangement high nitrogen stainless steel femoral stem is used as working electrode, Ag/AgCl electrode as reference electrode and platinum is used as counter electrode. The volume of the cell shall be between 5-100 mL. Electrochemical measurement is recorded using a PGSTAT 101 potentiostat with a scan rate of less than 1mV/sec. The corrosion software NOVA is used for data analysis and electrochemical control[32]. Corrosion current density (i_{corr}) and corrosion parameters i.e. anodic and cathodic Tafel slopes are obtained from the polarization curves by Tafel extrapolation technique. Detail experimental setup is already mentioned above in standard G5 [33].

Robert Wen et al mentioned that polarization curve for Ti-6Al-4V implant were recorded at E_{corr} value of +-250 mV at scan rate of 0.5 mV/s. At given scan rate within the range of -150 to +1000 to 2500 mV versus $E_{corr,}$ steady state polarization curves were observed [32]. Interestingly for Co-Cr-Mo implants the steady state curve were obtained in the potential range of -150 to +2000 mV versus E_{corr} at scan rate of 1 mV/s Electrochemical corrosion studies on Co-Cr-Mo by Yi Chen[32].

6. REAGENTS

6.1 Lubricants

Lubricants used within simulators should mimic natural lubricants found in vivo. The skeletal bearing of the hip joint is lubricated with synovial fluid, a dialysate of blood with the additional protein hyaluronic acid. Hyaluronic acid is secreted from the articular cartilage surrounding the epiphysis of the femur and acetabular cup of the pelvis[34]. It has been assumed that upon implantation of THA devices, the device is surrounded by a similar fluid,

however in the absence of articular cartilage it is unlikely that this fluid exactly replicates synovial fluid[34].

6.2 Conformity

The degree of conformity of bearings within modular devices can affect the lifespan and thus perceived success of an implant. This is more commonly referred to as the clearance of the hip joint which can be defined as the difference between the diameters of the acetabular cup and the femoral head[35]. Data from studies which have performed friction and wear simulations suggest that provided a substantial fluid film exists between the bearing interface friction is reduced as is bedding in wear after initial implantation: however the thickness of the fluid film is dependent on the angular velocity and viscosity of the fluid, thus elastohydrodynamic film thickness controls wear[36].

6.3 Lubrication Mechanisms

If the same is true of the taper interface where a high degree of conformity is expected the viscosity of the lubricating fluid must alter the wear rate of the two surfaces. SEM analysis of the taper interface support mixed lubrication followed by elastohydrodynamic lubrication between the head and taper which further supports work by D.Dowson [37][36]. Mixed lubrication involves both hydrodynamic lubrication and boundary lubrication mechanisms. In hydrodynamic lubrication separation of the two surfaces is complete thus the behaviour of the contact is determined by the physical properties of the lubricant and shearing of the viscous lubricant. Laws of dry friction apply to boundary lubrication as the coefficient of friction is independent of load speed and contact area, thus mixed lubrication involves a suggested mixture between the two extremes of lubrication[10]. Mixed lubrication may take place during the wearing in stage of the taper interface due to machining grooves of the taper as illustrated in Figure 6-1 below. SEM images of the taper surface after wear within the junction show shearing off of the machining grooves thus resulting in material loss at the taper surface[37].

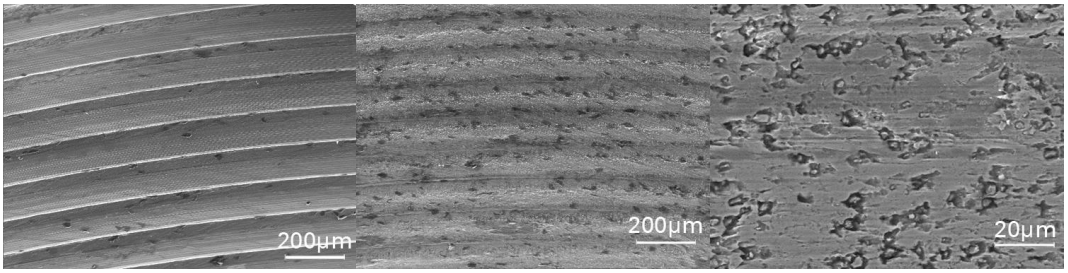

Figure 6-1. From left to right -SEM image of an unworn manufactured taper surface, SEM image of worn taper surface at the same magnification, SEM image of worn taper surface at a higher magnitude showing the presence of pits within the surface[37]**.**

6.4 Significance of Viscosity

An equation derived in 1978 by B Hamroek and D.Dowson has been modified in order to calculate the film thickness as a term of head diameter, see equation 2.2 [38] Where $h_{min}$is the minimum film thickness, d is the spherical head diameter and $c_d$is the diametral clearance[36] [38].

$$\boldsymbol{h_{min} = 1.6904 \times 10^{8} \frac{d^{2.19}}{{c_d}^{0.77}}} \qquad \text{Equation 3.2.3.1}$$

In order to calculate this the lubricant viscosity, femoral head diameter, angular velocity and cyclic load were used[38]. Although this is a useful equation it applies only to the geometries of the femoral head and acetabular cup in hip replacements and thus cannot be used to determine the degree of clearance within the taper interface.

6.5 Procedure

Fluid viscosity is an important physical property of fluid between load bearing contacts as viscosity determines the thickness of the separating film between the bearing surfaces and thus the degree of wear and load carrying capacity[39]. The viscosity of each fluid was taken using a novel experimental ultrasonic technique for measuring viscosity in real time. When an ultrasonic wave is directed on a solid liquid interface the proportion of the wave that is reflected is related to the viscosity of the liquid[39], see Figure 6-2. A shear wave at 10^6 (s^{-1}) was used, this shear is known to be experienced between the acetabular cup and femoral head during normal walking, although the shear experienced within the taper interface is unknown. It is anticipated that the shear rate within the contact will determine the viscosity of the liquid within the interface and thus affect the wear rate and separation of the taper from the head.

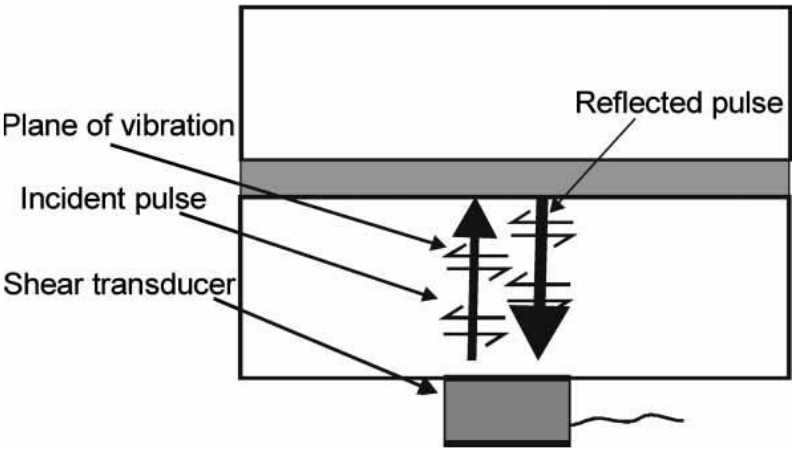

Figure 6-2: Schematic diagram of shear wave ultrasonic measurement of viscosity of a thin fluid film[39].

6.6 Fluids and ASTM F1875

Proteinacious fluid suggested within the ASTM-1875f standard is recommended to 'best simulate the in-vivo environment' in method 1. While the use of the proteinacious solution goes some way in replicating the exposure of the taper interface in vivo it could be argued that 10% FCS in 0.9%NaCL wt% in distilled water is inadequate. Additionally ISO 14242-1-2002, 'Implants for surgery – Wear of total hip joint prosthesis' uses 25%FCS with 0.9%NaCl in distilled water as a lubricant in a hip simulator[40]. Considering the previous point regarding the conformity of the device, and the factors affecting the extent of wear the viscosity of each solution was measured using an ultrasonic method.

6.7 Results

The effect of NaCl on serum was also deemed of interest thus the following solutions were analysed, the table below presents the viscosity measurements however it must be noted that verification of these results must be validated with the use of a high shear rheometer. Due to the non-Newtonian behaviour of calf serum the fluid should be analysed at various shears in order to compose a full understanding of the fluids viscoelastic properties, along with effects from shear thinning.

Table 6-1: Table of viscosity results obtained by an ultrasonic shear wave device

Solution	Viscosity (mPas) at 19℃
10% FCS +0.9% NaCl	1.62
10% FCS + PBS	1.64
25% FCS +NaCl	1.52
25% FCS + PBS	1.81
100% FCS	1.22
100% NaCl	1.32
100% PBS	1.10

6.8 Discussion

Previous analysis on synovial fluid has indicated the tendency of the non-Newtonian fluid to exhibit shear thinning, as suggested the viscosity of the fluid decreases with increased shear rate[10]. This may explain why the viscosities of each fluid do not vary significantly. As solutions have only been tested at high shear rates, 10^6 (s^{-1}) most solutions tend towards 1mPas, which is similar to the viscosity of water at 1 mPas [10].

7. OPTICAL MICROSCOPY

7.1 Literature Review

A fretting rig which uses radiotracers has been developed by Schaaff et al to investigate fretting wear in cobalt chromium against titanium alloy. As part of that study they determined that machining marks were present on the surfaces even after mechanical polishing, these were visible through optical microscopy, see Figure 7-1. By conducting optical microscopy prior to testing they were able to determine which marks were due to machining and thus could exclude these from images taken after testing. [41]

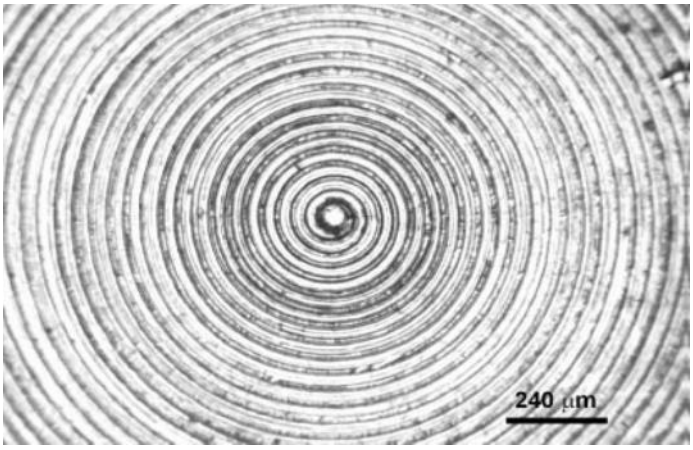

Figure 7-1 - An optical microscopy image of marks caused by mechanical polishing [26].

Dalmiglio et al also found evidence of post-polishing machining marks. However they state that roughened surfaces can have less fretting wear. This can be used to explain the threading observed on the implants acquired for testing. [42]

Varenberg et al performed a ball on plate fretting test, without a medical focus, which they analysed using optical microscopy. When presenting their results a detailed description of what wear mechanisms caused which parts of the image was provided. It is claimed that very bright portions of the image correspond to wear debris, as the surface is higher there than for the rest of the image. It is also explained that the dark regions are areas where wear has occurred, as the surfaces are farther away there. If these occur in "clumps" it is probable that the primary wear mechanism is adhesion and the debris has been released by fretting fatigue. If there are light and dark lines it is probable that the main wear mechanism has been abrasion. Figure 7-2 and Figure 7-3 explain this more clearly. [43]

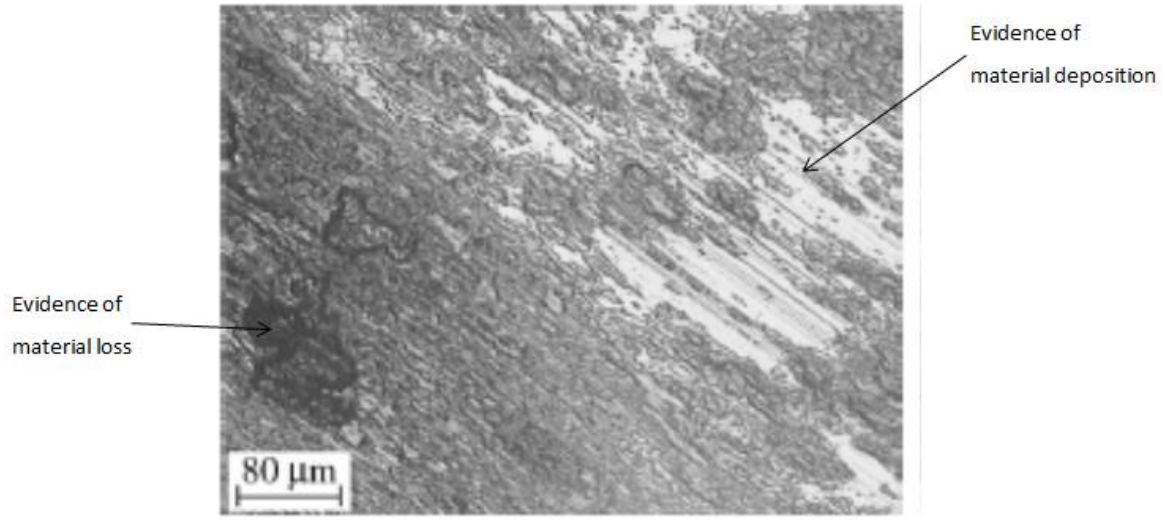

Figure 7-2-An optical microscopy image showing adhesive wear [43]

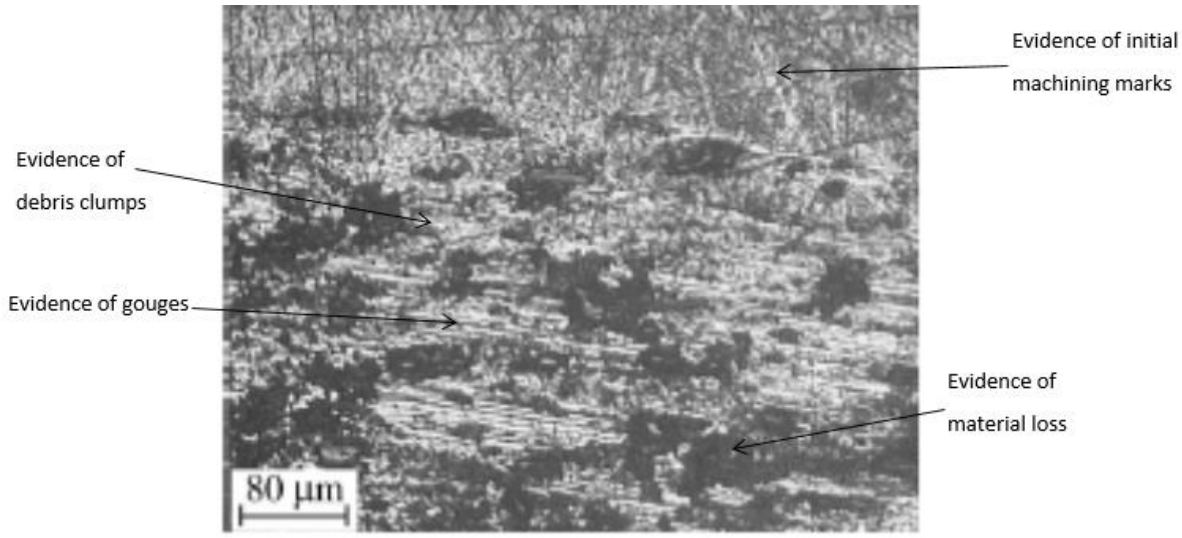

Figure 7-3 - An optical microscopy image showing abrasive and adhesive wear and machining marks. [43]

7.2 Methods

- Prepare the leica microscope table. Ensure the specimen area is clear from debris and the light source is not obstructed.
- Switch on the microscope. The specimen table should begin moving to ensure full motion is available.
- Start the program (LAS V3.8).

- Place the specimen on a clear mounting block and ensure approximate target area is above light source.
- Select the “MIC 1” tab on the left side of the screen.
- Ensure the camera option has been selected to provide a display on the computer.
- Select the “camera” tab, also on the left side of the screen.
- Ensure the “wheel” icon is selected, as this auto adjusts the exposure amount and set the image type to greyscale.
- Next select the “z stack” option to define the limit of the multi-focus image.
- Select the arrow next to the “Start” and using the rear dial on the control pad adjust the table height to the point a region of the image begins to focus.
- Then select the arrow next to the “End” and, again using the rear dial, lower (or higher depending on the “Start” arrow position) until the entire image has been in focus (it does not still have to be focused).
- Then select “Acquire multifocus” and wait whilst the microscope automatically adjusts the table height, acquiring images in steps, and compiles them.
- When a completed image has been approved (if the limits were incorrect the image may not be in focus and may have to be repeated) post-editing can be done.
- For this methodology a scale bar is required:
- Select the icon at the top of the panel on the right of the screen, with a scale bar image on it.
- Then adjust the settings of the scale bar as required, for example: a font size of 72, a line thickness of 10, a black background and positioning in the right bottom corner.

7.3 Results

7.3.1 Explant Image

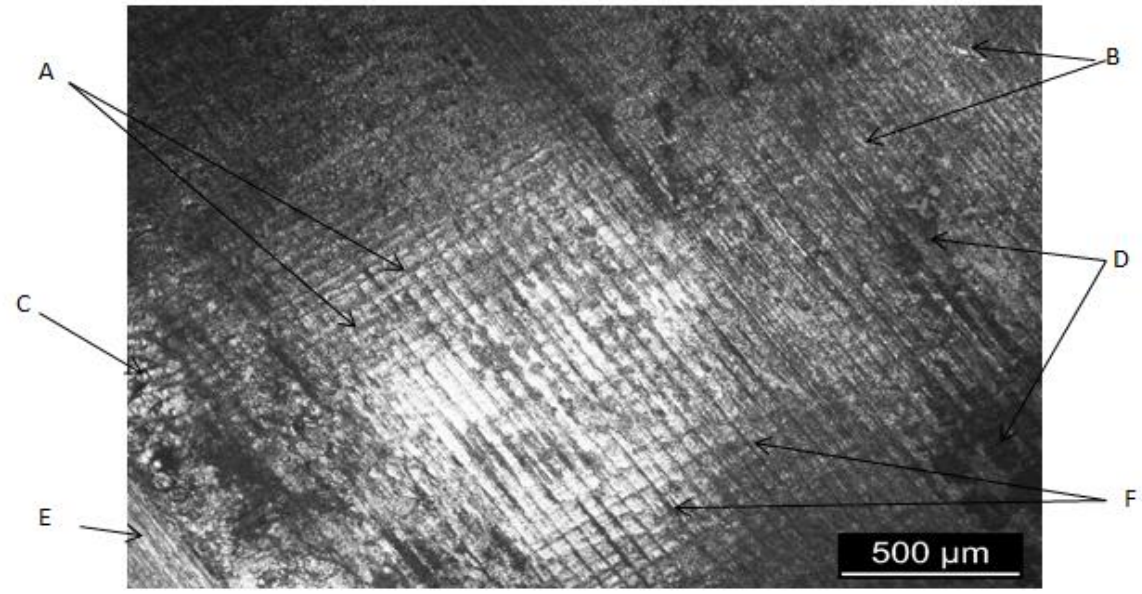

Figure 7-4: An optical microscope image of the taper base from the 1 year retrieved implant

Table 7-1: A table to accompany Figure 7-4

Marker	Evidence	Form of wear
A	Longitudinal striations	Abrasive
B	Wear debris	Adhesive
C	Large Debris Conglomeration (at edge of head contact)	Adhesive & Abrasive
D	Material loss	Adhesive
E	Machining marks, evidence of initial surface texture	N/A
F	Circumferential striations	Abrasive

7.3.2 Coupon Image

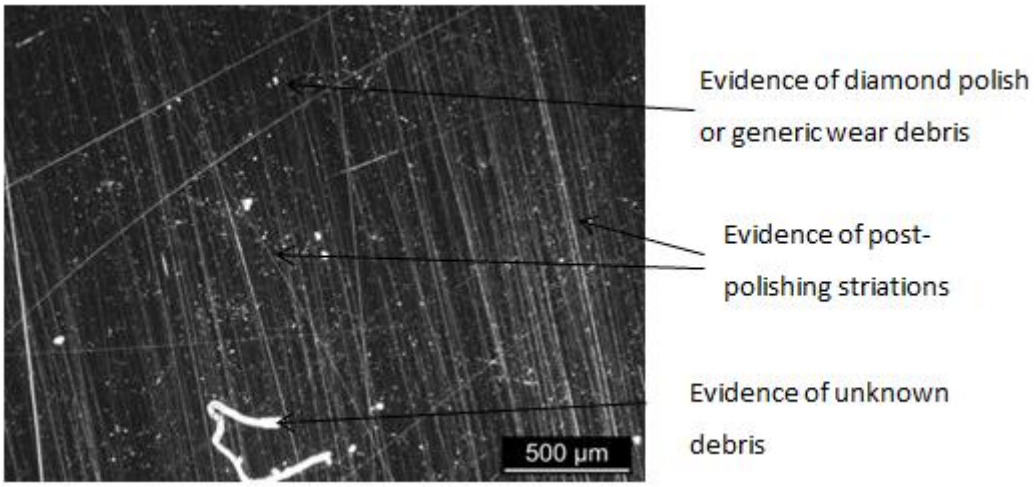

Figure 7-5: An optical microscopy image of a post-polished coupon surface

7.4 Discussion

7.4.1 Explants

Figure 7-4 shows evidence of micromotion from the taper tip to the taper base, it is the only one of the explant images to display such abrasion so clearly. The image taken from the other side of the same implant at the same location had only minor evidence of striations in that orientation. This could indicate a slight unbalanced motion, similar to a "wobble", where the head moves more on one side than the other. If this is a common in vivo occurrence it is not replicated in the testing method from ASTM 1875 and so perhaps the standard would be incorrect. An alternative explanation would be poor surgical implantation.

Images taken at the taper tip show primarily circumferential striations, which could have been caused by machining prior to implantation. [28]. There is also some evidence on one side of the 8.7 year retrieval of adhesion occurring on the chamfer edge. This can be explained by unbalanced loading, with one side taking more load than the other, resulting in increased probability of cold wearing occurring. This could have been caused by poor implantation. An alternative explanation s damage occurring during retrieval.

7.4.2 Coupons

All of the coupons were imaged after polishing, where they were ground and polished to a 0.25µm surface finish. This surface finish is colloquially referred to as "mirror finish" and as

such is considered to be near perfect. Having taken optical microscopy images it can be seen that this is not the case, as evidenced in Figure 7-5. This post-polishing imperfection would be found on the tapers that have been provided and indicate the benefit of pre-testing images being taken.

It can be seen in Figure 7-5 that an unknown piece of debris was present. It was initially believed that this was a hair, however prior to the image being fixed efforts were made to remove the debris from microscope table. These were unsuccessful and so the image was taken. After the microscopy was concluded a visual examination of the coupon was undertaken and a small, adhered, piece of material could be seen. The debris has a similar appearance to the resin the sample was mounted in and so it is assumed that the debris is an errant piece of ceramic. This could affect the results if it became dis-lodged as it would cause third body wear.

8. SCANNING ELECTRON MICROSCOPY

8.1 Scanning Electron Microscope and Energy Dispersive X-ray Spectroscopy

A Carl Zeiss Evo SEM, seen in Figure 8-1 below, was used to analyse various explants as the SEM analysis method produces high resolution and high magnification images.

Figure 8-1: Carl Zeiss Evo scanning electron microscope used in this investigation.

SEM produces images by scanning the sample using a focused beam of electrons, which interact with the atoms of the sample. Due to this interaction between the beam of electrons and the atom, secondary electrons (SE), back-scattered electrons (BSE) and characteristic X-

rays are produced. When the high energy electrons from the SEM beam contact the sample, inner shell electrons of the sample develop higher energy states and therefore an outer shell electron which has a higher energy will replace the electron in the inner shell. This change of energy states causes an emission of an X-ray of equal wavelengths to that of the element. EDX is a method in which the emitted X-rays are used to determine the elemental composition and elemental abundance of the specimen[44].

8.2 Results

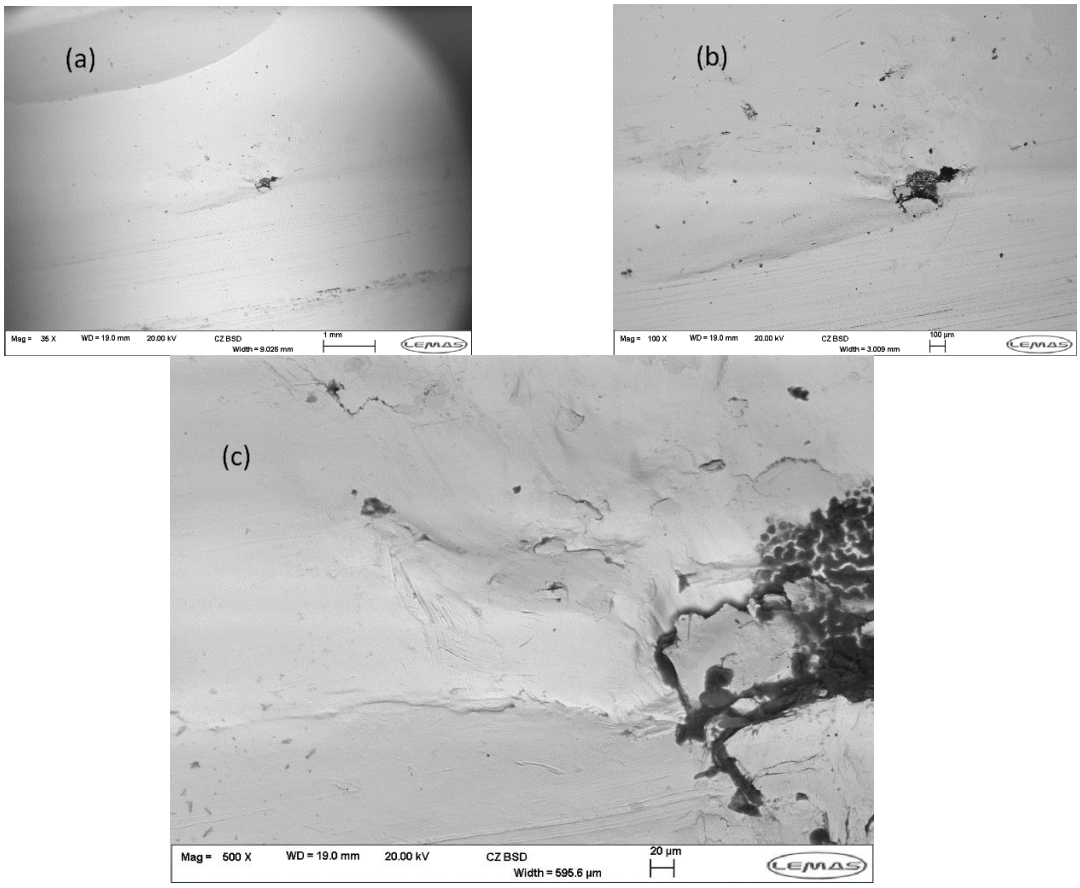

Figure 8-2: SEM images of sample taper of 8.7 year explant showing wear scar, (a) at 35x, (b) at 100x and (c) at 500x magnification

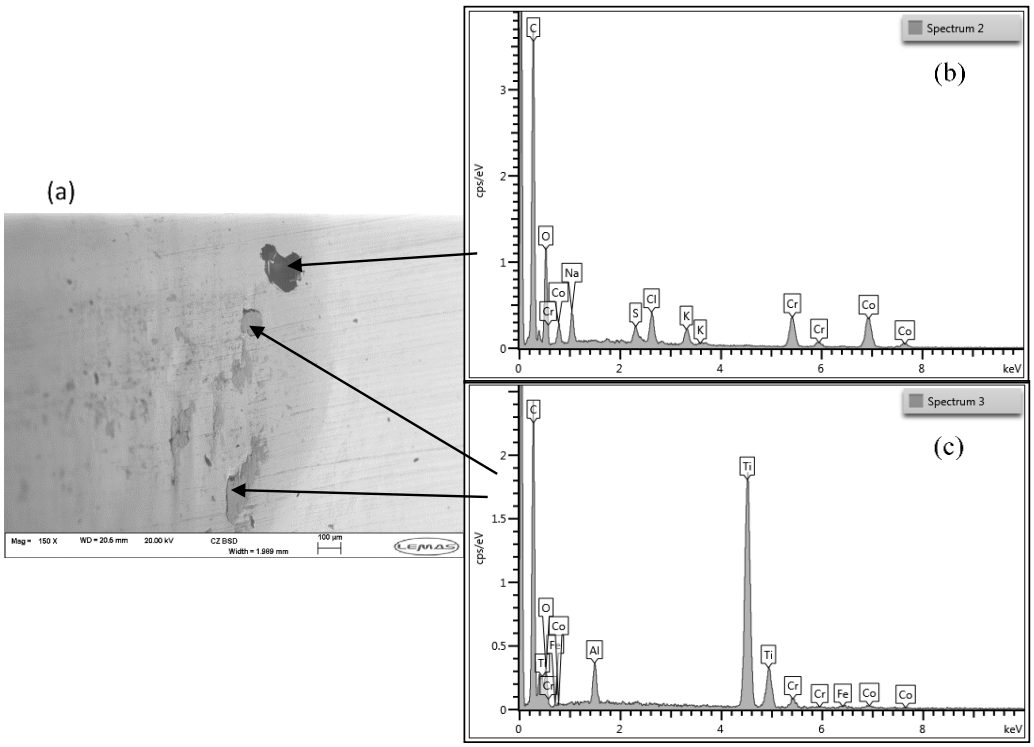

Figure 8-3: (a) SEM image of on sample taper of 8.7 year explant along with (b), (c) EDX spectrum at various spot

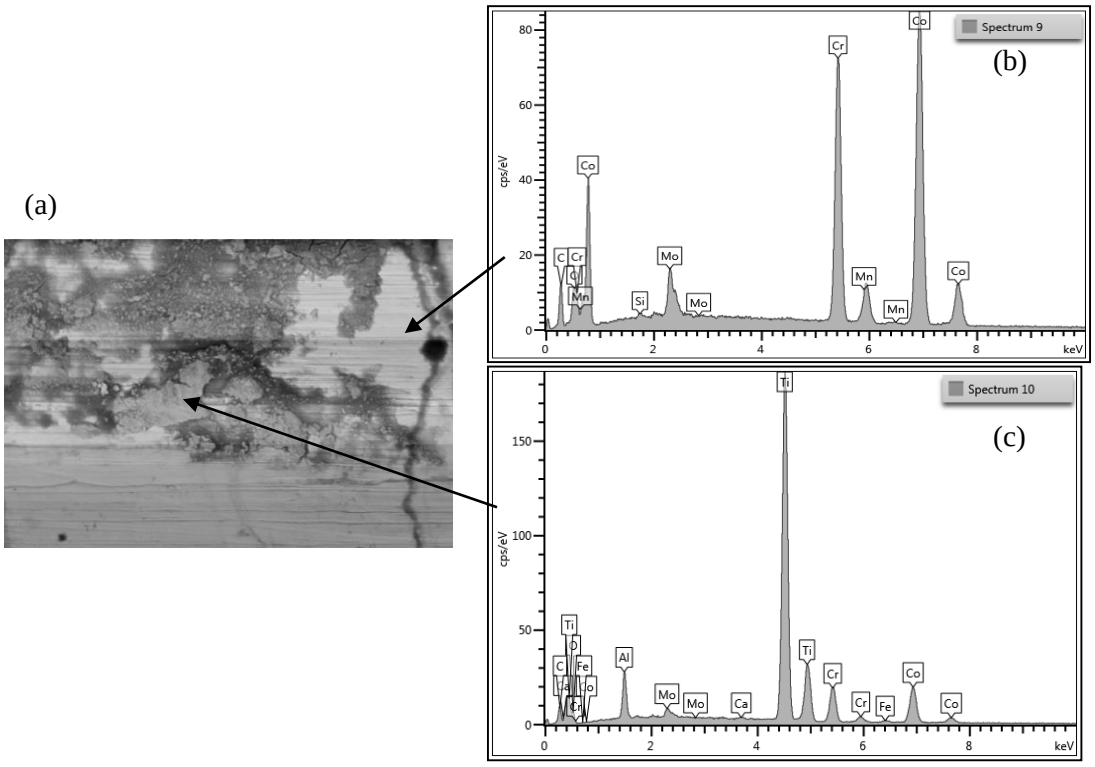

Figure 8-4: (a) SEM image of on sample taper of 8.7 year explant along with (b), (c) EDX spectrum at various spot

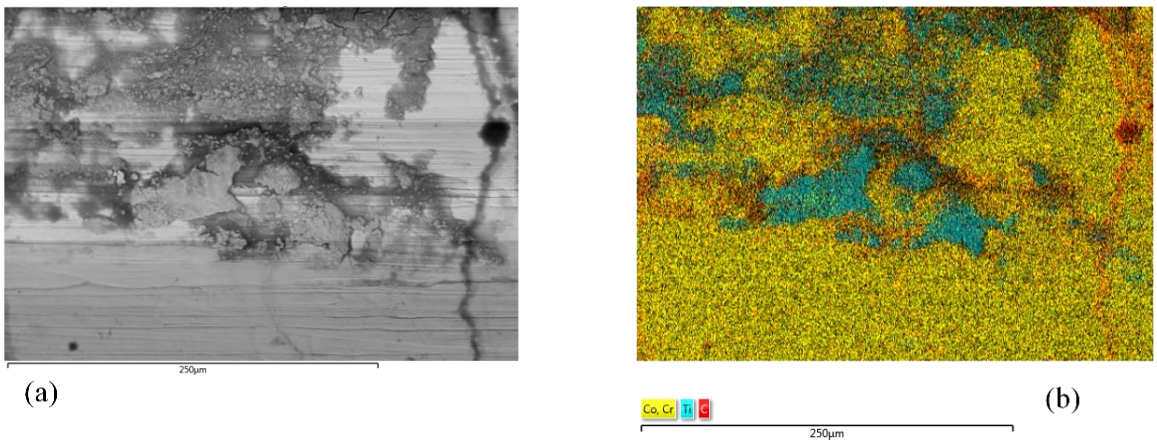

Figure 8-5: (a) SEM image of on sample taper of 8.7 year explant and (b) EDX mapping of Co, Cr (yellow); Ti (blue) and C (red).

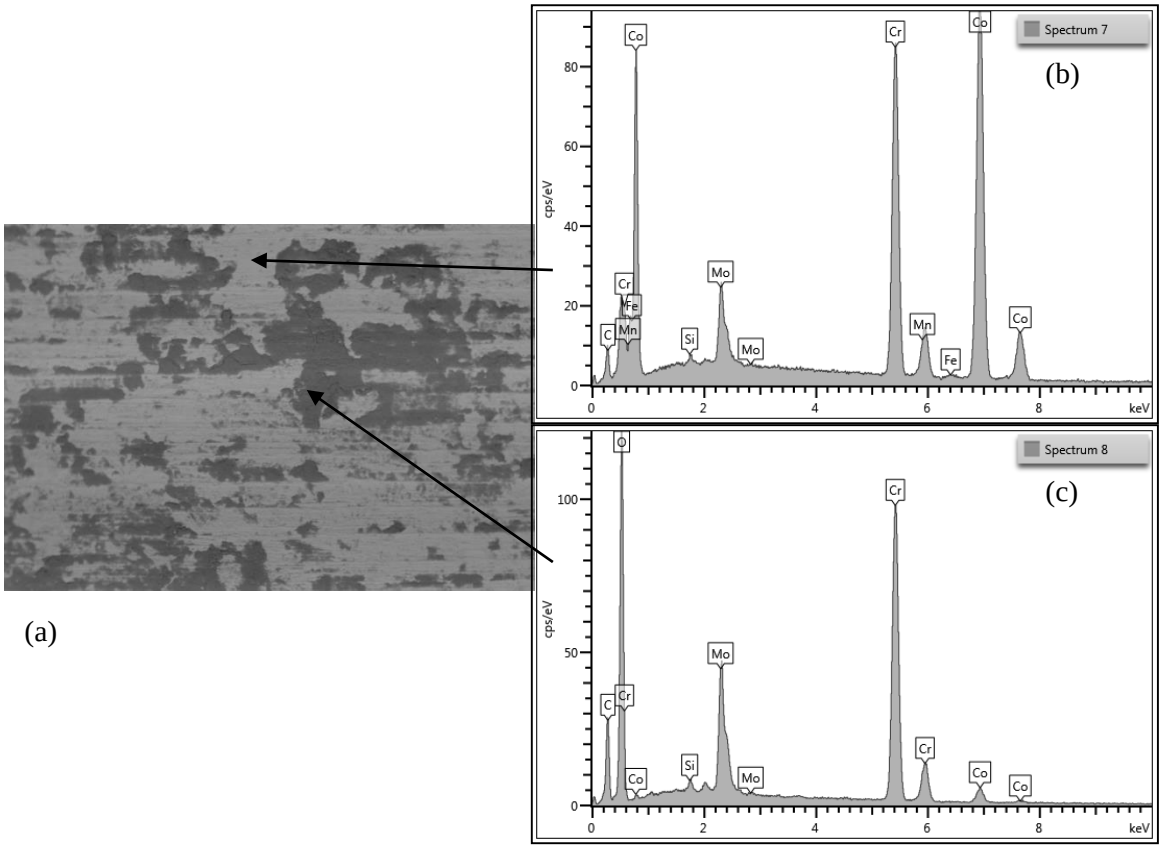

Figure 8-6: (a) SEM image of on sample taper of 1 year explant along with (b), (c) EDX spectrum at various spot

8.3 Discussion of SEM and EDXS

Scanning electron microscopy and energy dispersive X-ray spectroscopy were performed on various sections of the taper stems of two explants. SEM images are useful for such investigations as they can be used to compare to optical microscopy images and rule out possible assumptions from the optical microscopy analysis. Both explant stems were made of cobalt chrome, CoCr and this was shown using EDXS analysis and can be seen on the EDXS spectrums in Figure 8-4 and Figure 8-6. On the SEM images, some horizontal markings can be seen which are likely lay leftover from machining.

It can be seen from Figure 8-2, a region of the taper has been deformed, which is due to the wearing of the taper due to its contact with the femoral head. The characteristics of the regions seen in Figure 8-2-c and Figure 8-5-a also suggest that there has been localised corrosion on the taper. Organic matter such as protein or blood denature to carbon and may be seen in the SEM images. Darker regions within SEM indicate elements with lower atomic mass, such as carbon, and therefore it can be presumed that the darker regions, especially

within Figure 8-2 and Figure 8-3 are organic matter such as dried blood. This can further be analysed using the EDXS spectrum seen in Figure 8-3. It can be seen from Figure 8-3-b that the dark spot on the sample has a high abundance of carbon.

The energy dispersive X-ray spectrums in Figure 8-3-c and Figure 8-4-c show that there is a high amount of titanium Ti on the taper. From the EDXS spectrum, it can be assumed that the femoral head or acetabular cup had deposited the material onto the taper, whilst in contact with the stem. It can be seen from Figure 8-3-c and Figure 8-4-c that other materials such as aluminium Al and vanadium V were also present in the region and deposited onto the stem when in contact with the other components. Figure 8-5-b is an EDXS mapping image which shows the traces of Ti at a wear scar on the taper.

SEM and EDXS were also performed on a 1 year explant, but no regions of wear were found. However point EDXS analysis from regions of this taper showed areas with a high abundance of chromium Cr and oxygen O, which can be seen in Figure 8-6-c. The traces of O suggests the oxidation of the surface of the taper and possible film formation.

9. CRITIQUING ASTM F1875

ASTM F1875 is intended to provide a benchmark set of tests which manufacturers can use to quickly compare design iterations. It is not intended to simulate the conditions of the in vivo environment completely. The standard also states it is hoped researchers can compare results more readily if they test under the same set-up and conditions. As Neu states in his review "Progress in standardization of fretting fatigue terminology and testing", ASTM F1875 is an ASTM *standard practice* rather than an ASTM *standard test method*, meaning it is guidance rather than a absolute test methodology [45].

Nevertheless, the overall structure of the standard could be set out far more clearly. Essentially two test methods are suggested. Method I uses either full modular hip components or representative test coupons in an upright orientation, but mounted at an angle of 10° off the loading axis (as per ASTM F1440). Mounting according to ASTM F1440 leaves a significant proportion of the stem unsupported, which may incur unnecessary bending moments and associated stresses. Method I does not use electrochemistry but suggests a total elemental level analysis to capture all ions and particulate debris present in a tested solution (it is purported other analytical techniques fail to differentiate between ions and particulates). Method I also specifies a qualitative inspection of taper surfaces for fretting wear by optical

microscopy and a quantitative measure of damage from the total elemental analysis SEM provides. Method I uses a proteinaceous solution of 10% calf serum in 0.9% NaCl in distilled water. Method II also uses either full modular hip components or representative test coupons but in an inverted orientation, but comprehensive details of the test rig set-up are not provided, for example mounting angles relative to the loading axis are not specified and no fixturing method suggested. A seal is specified between the femoral head and the load application surface, presumably to prevent corrosion here which would draw corrosion away from the region of interest; the taper interface. However it is not clear why the components must be inverted, as this actually makes design of a seal more difficult. Method II uses electrochemistry, but states this will require validation by elemental analysis for tests of mixed metal devices. Method II uses an electrolyte solution of 0.9% NaCl in distilled water.

Testing methodologies for the two methods is not made clear. Under heading "9 Procedure", Section 9.1 of the standard is titled simply "Test Method". The section specifies loading values, test frequency and test duration. Further down, section 9.2 is titled "Test Method II" and details a different loading procedure, test frequency and test cut-off criteria. It is therefore assumed section 9.1 is referring to Method I and should be titled as such.

A definitive method of attaching heads to stems and later removing them at consistent angles and forces should be referenced, for example ASTM F2009 or ISO 7206-10.

ASTM F1875 fails to specify handling practices for implants during testing. It should be stated in the procedure that implants should always be handled with latex-free gloves as grease from human skin can affect the electrochemistry results of tests. It does state proteinaceous solutions risk microbial contamination, so Method I tests should be carried out under sterile conditions. The standard should also specify that materials for the test rig's design should be inert and not affect either corrosion or electrochemical analyses, e.g. only polymers may be in contact with the test solution, not metals.

The loading forces and frequencies chosen to load the specimen in ASTM F1875 seem arbitrary. Bergmann et al measured contact forces in four patients when doing different activities [18]. They find walking load cycles between 200-1800N on average at an average frequency of 0.91Hz.

Changing the loading procedure has been found to reveal more information about fretting corrosion mechanisms. For example stainless steel stems were tested with CoCr heads by Gilbert et al. They increased cyclic load at 3Hz by 100N increments, starting at 100N to

1000N, then increased load by 200N increments up to 3300N, and found the fretting corrosion onset load was 900N - lower than the CoCr/CoCr material pair they also tested [24]. Variable loading was also explored in an earlier paper by Goldberg and Gilbert which had previously found loads lower than those induced by walking were enough to cause fretting [2].

10. CONCLUSIONS

10.1 Rig Design

After reviewing the literature for similar tests using similar materials, testing parameters have been chosen for a ball-on-flat tribocorrosion test. This will enable fast analysis of fretting-corrosion between the material pair investigated in a more controlled environment than the ASTM F1875 compliant tests.

Two test rigs have been designed and are being manufactured in accordance with the two test methods that ASTM F1875 specifies. A fixturing method is yet to be designed and manufactured for positioning modular stems and heads at consistent angles when assembling and disassembling these modular components.ASTM F1875 has been analysed and critiqued, but the procedures are yet to be scrutinised in a testing environment.

10.2 Reagents

Synovial fluid has specific characteristics and is a complex fluid to characterise due to its composition and non-Newtonian behaviour. A greater understanding of proteins and compounds within FCS must be understood in relation to tribocorrosion and also interactions with wear debris in order to allow a greater understanding of wear mechanics within the taper interface to be addressed. In vivo analysis of the viscosity of synovial fluid could prove to be a useful property to quantify when considering skeletal joint diseases as a prediction of pathology and degenerative time scales and severity. Viscosity considerations of synthetic synovial fluid could help further develop more realistic THA simulations of healthy and diseased joints; However further studies are required to evaluate this.

10.3 Optical Microscopy and SEM

Optical microscopy techniques are not superfluous if SEM is also used as imaging techniques of the tapers. Optical microscopy offers useful information of wear marks regarding their orientation and position on the taper, along with enabling identification of regions of greater extent of wear. SEM additionally allows these regions to be analysed in more depth, providing a valuable insight into adhesion wear mechanisms and also wear clarification of discoloured regions.

11. FUTURE WORK

Potential areas for future work include the completion of Method 1 and 2 as described by the ASTM-1875 standard, by doing so further analysis of electrochemical methods, fretting regimes and the effect of different solution properties could be verified.

11.1 Ball on Plate Test

- Define suitable parameters.
- Assess variants in fluids in order to test the solutions used in ASTM 1875, and to reiterate any differences found within the fretting rig designs in Method 1 and 2 of ASTM 1875
- Make a comparison of fretting rate of materials.

11.2 ASTM F1875-98

- Assess any difference between the upright and inverted rig.
- Vary loads and number of cycles to explore fretting corrosion between this taper and head.
- Investigate the effect of varying parameters (suggested loads between ASTM methods vary from 3000N to 2000N) suggested in ASTM 1875.
- Complete fretting simulation and continually assess fluid properties to find any difference in fretting mechanisms.
- Assessment of the effect of fluid viscosity on the simulation and also the effect of viscosity on fretting.

REFERENCES

[1] I. Caminha and C. Roesler, “Evaluation of the fretting corrosion mechanisms on the head-cone interface of hip prostheses,” *Mater. ...*, vol. 72, pp. 77–84, 2011.

[2] J. R. Goldberg and J. L. Gilbert, “In Vitro Corrosion Testing of Modular Hip Tapers,” pp. 78–93, 2002.

[3] ASTM, “ASTM F1875 − 98 Standard Practice for Fretting Corrosion Testing of Modular Implant Interfaces : Hip Femoral Head-Bore and Cone Taper Interface,” 2009.

[4] E. Dall’Ara, C. Ohman, M. Baleani, and M. Viceconti, “Reduced tissue hardness of trabecular bone is associated with severe osteoarthritis.,” *J. Biomech.*, vol. 44, no. 8, pp. 1593–8, May 2011.

[5] U. Holzwarth and G. Cotogno, *Total Hip Arthroplasty: State of the Art, Challenges and Prospects*, no. July. European Commission Joint Research Centre, 2012, p. 62.

[6] D. C., “THE CHARNLEY TOTAL HIP REPLACEMENT.” .

[7] N. Wishart, R. Beaumont, E. Young, V. Mccormack, and M. Swanson, “National Joint Registry 11th Annual Report,” 2014.

[8] M. P. Chairman, R. Beaumont, E. Young, O. Forsyth, and M. Swanson, “10th Annual Report,” *Natl. Jt. Regist.*, no. December 2012, 2013.

[9] “Zimmer Hip Replacement Implants,” *Healthbase Medical Tourism Resources Site*, 2015. .

[10] Prof. M. Priest, “Introduction to Tribology. Work Unit 2. Friction and Wear of Surfaces,” 2014.

[11] a Buford and T. Goswami, “Review of wear mechanisms in hip implants: Paper I – General,” *Mater. Des.*, vol. 25, no. 5, pp. 385–393, Aug. 2004.

[12] S. Mischler, “Triboelectrochemical techniques and interpretation methods in tribocorrosion: A comparative evaluation,” *Tribol. Int.*, vol. 41, no. 7, pp. 573–583, Jul. 2008.

[13] D. Landolt, S. Mischler, and M. Stemp, “Electrochemical methods in tribocorrosion: a critical appraisal,” *Electrochim. Acta*, vol. 46, no. 24–25, pp. 3913–3929, Aug. 2001.

[14] S. W. Watson, F. J. Friedersdorf, B. W. Madsen, and S. D. Cramer, “Methods of measuring wear-corrosion synergism,” *Wear*, vol. 181–183, pp. 476–484, Mar. 1995.

[15] J. Fisher, D. Dowson, and R. Cooper, “The effect of transfer film and surface roughness on wear of lubricated untra-high molecular weight polyethylene,” *Clin. Mater.*, vol. 14, pp. 295–302, 1993.

[16] Y. Yan, A. Neville, and D. Dowson, “Biotribocorrosion of CoCrMo orthopaedic implant materials—Assessing the formation and effect of the biofilm,” *Tribol. Int.*, vol. 40, no. 10–12, pp. 1492–1499, Oct. 2007.

[17] M. Baxmann, S. Y. Jauch, C. Schilling, W. Blömer, T. M. Grupp, and M. M. Morlock, “The influence of contact conditions and micromotions on the fretting behavior of modular titanium alloy taper connections.,” *Med. Eng. Phys.*, vol. 35, no. 5, pp. 676–83; discussion 676, May 2013.

[18] G. Bergmann, F. Graichen, a Rohlmann, a Bender, B. Heinlein, G. N. Duda, M. O. Heller, and M. M. Morlock, “Realistic loads for testing hip implants.,” *Biomed. Mater. Eng.*, vol. 20, no. 2, pp. 65–75, Jan. 2010.

[19] S. Barril, S. Mischler, and D. Landolt, “Influence of fretting regimes on the tribocorrosion behaviour of Ti6Al4V in 0.9wt.% sodium chloride solution,” *Wear*, vol. 256, no. 9–10, pp. 963–972, May 2004.

[20] D. He, T. Zhang, and Y. Wu, “Fretting and galvanic corrosion behaviors and mechanisms of Co – Cr – Mo and Ti – 6Al – 4V alloys,” vol. 249, pp. 883–891, 2002.

[21] M. J. Runa, M. T. Mathew, and L. a. Rocha, “Tribocorrosion response of the Ti6Al4V alloys commonly used in femoral stems,” *Tribol. Int.*, vol. 68, pp. 85–93, Dec. 2013.

[22] N. Diomidis, S. Mischler, N. S. More, and M. Roy, “Tribo-electrochemical characterization of metallic biomaterials for total joint replacement.,” *Acta Biomater.*, vol. 8, no. 2, pp. 852–9, Feb. 2012.

[23] T. Zhang, N. M. Harrison, P. F. McDonnell, P. E. McHugh, and S. B. Leen, “A finite element methodology for wear–fatigue analysis for modular hip implants,” *Tribol. Int.*, vol. 65, pp. 113–127, Sep. 2013.

[24] J. L. Gilbert, M. Mehta, and B. Pinder, “Fretting crevice corrosion of stainless steel stem-CoCr femoral head connections: comparisons of materials, initial moisture, and offset length.,” *J. Biomed. Mater. Res. B. Appl. Biomater.*, vol. 88, no. 1, pp. 162–73, Jan. 2009.

[25] J. R. Goldberg, C. A. Buckley, J. J. Jacobs, and J. L. Gilbert, “Corrosion testing of modular hip implants,” *Modul. Orthop. Implant.*, vol. 1301, pp. 157–176, 1997.

[26] S. C. Jani, W. L. Sauer, T. W. Mclean, R. D. Lambert, and P. Kovacs, “Fretting Corrosion Mechanisms At Modular Implant Interfaces,” in *Symposium on Modularity of Orthopedic Implants, ASTM STP 1301*, 1997, pp. 211–225.

[27] N. J. Hallab, C. Messina, A. Skipor, and J. J. Jacobs, “Differences in the fretting corrosion of metal-metal and ceramic-metal modular junctions of total hip replacements.,” *J. Orthop. Res.*, vol. 22, no. 2, pp. 250–9, Mar. 2004.

[28] P. Schaaff, W. Horstmann, M. Dalmiglio, and U. Holzwarth, “A compact fretting device for testing of biomaterials by means of thin layer activation,” *Wear*, vol. 261, no. 5–6, pp. 527–539, Sep. 2006.

[29] M. G. Bryant, “FRETTING-CREVICE CORROSION OF CEMENTED METAL ON METAL TOTAL HIP REPLACEMENTS,” 2013.

[30] ASTM, “ASTM F1440 − 92 Standard Practice for Cyclic Fatigue Testing of Metallic Stemmed Hip Arthroplasty Femoral Components Without Torsion 1,” vol. 92, pp. 1–6, 1992.

[31] M. Lgried, T. Liskiewicz, and A. Nevvile, “Electrochemical Investigation of corrosion and wear interactions under fretting conditions,” *Wear*, pp. 52–58, 2012.

[32] R. W.-W. Hsu, C.-C. Yang, C.-A. Huang, and Y.-S. Chen, “Investigation on the corrosion behavior of Ti–6Al–4V implant alloy by electrochemical techniques,” *Mater. Chem. Phys.*, vol. 86, no. 2–3, pp. 269–278, Aug. 2004.

[33] E. J. Rebek, “G5,” vol. 36. Oct-2011.

[34] A. . Cooke, D. Dowson, and V. Wright, “The rheology of synovial fluid and some potential synthetic lubricants for degenerate synovial joints.,” *Eng. Med.*, vol. 7, no. 66, pp. 66–72, 1978.

[35] X. Q. Hu, R. J. K. Wood, a. Taylor, and M. a. Tuke, “The tribological behaviour of different clearance MOM hip joints with lubricants of physiological viscosities,” *Proc. Inst. Mech. Eng. Part H J. Eng. Med.*, vol. 225, no. 11, pp. 1061–1069, Sep. 2011.

[36] D. Dowson, “Tribological principles in metal-on-metal hip joint design,” *Proc. Inst. Mech. Eng. Part H J. Eng. Med.*, vol. 220, no. 2, pp. 161–171, Jan. 2006.

[37] D. J. Langton, R. Sidaginamale, J. K. Lord, A. V. F. Nargol, and T. J. Joyce, “Taper junction failure in large-diameter metal-on-metal bearings,” vol. 1, no. 4, pp. 56–63, 2012.

[38] B. J. Hamroek and D. Dowson, “Elastohydrodynamic Lubrication of Elliptical Contacts for Materials of Low Elastic Modulus I — Fully Flooded Conjunction,” vol. 100, no. April, 1978.

[39] S. Kasolang and R. S. Dwyer-Joyce, “Viscosity measurement in thin lubricant films using shear ultrasonic reflection,” *Proc. Inst. Mech. Eng. Part J J. Eng. Tribol.*, vol. 222, no. 3, pp. 423–429, May 2008.

[40] B. S. Iso, “Implants for surgery — Wear of total hip-joint prostheses —,” 2002.

[41] P. Schaaff, M. Dalmiglio, and U. Holzwarth, “Frequency effect in fretting wear of Co-28Cr-6Mo versus Ti-6Al-4V implant alloys.,” *J. Biomed. Mater. Res. B. Appl. Biomater.*, vol. 77, no. 1, pp. 79–88, Apr. 2006.

[42] M. Dalmiglio, P. Schaaff, U. Holzwarth, R. Chiesa, and G. Rondelli, “The effect of surface treatments on the fretting behavior of Ti-6Al-4V alloy.,” *J. Biomed. Mater. Res. B. Appl. Biomater.*, vol. 86, no. 2, pp. 407–16, Aug. 2008.

[43] M. Varenberg, G. Halperin, and I. Etsion, “Different aspects of the role of wear debris in fretting wear,” *Wear*, vol. 252, no. February, pp. 902–910, 2002.

[44] Geochemical Instrumentation and Analysis, “Scanning Electron Microscopy (SEM),” *Science Education Resource Center*, 2013. [Online]. Available: http://serc.carleton.edu/research_education/geochemsheets/techniques/SEM.html. [Accessed: 14-Jan-2015].

[45] R. W. Neu, “Progress in standardization of fretting fatigue terminology and testing,” *Tribol. Int.*, vol. 44, no. 11, pp. 1371–1377, Oct. 2011.